Master's thesis

NTNU
Norwegian University of Science and Technology
Faculty of Engineering
Department of Energy and Process Engineering

Martine Walvik Gundersen

Modelica Emulator for MPC Applications in Buildings

Master's thesis in Energy and Environmental Engineering
Supervisor: Laurent Georges
Co-supervisor: Harald Taxt Walnum and Igor Sartori
June 2021

NTNU
Norwegian University of
Science and Technology

Martine Walvik Gundersen

Modelica Emulator for MPC Applications in Buildings

Master's thesis in Energy and Environmental Engineering
Supervisor: Laurent Georges
Co-supervisor: Harald Taxt Walnum and Igor Sartori
June 2021

Norwegian University of Science and Technology
Faculty of Engineering
Department of Energy and Process Engineering

NTNU
Norwegian University of
Science and Technology

Summary

Buildings contribute to the world's energy consumption and greenhouse gas emissions. In order to reduce the energy use in buildings, it has been suggested to implement advanced control strategies of existing buildings. Among these control strategies, model predictive control (MPC) can be a promising option. Previous research on model predictive control has illustrated the energy saving potential of introducing said controls to existing buildings, but model predictive controls need to be optimized for the building in question. In order to benchmark, compare and experiment on the control algorithms offline, a simplified emulator of an office building in Oslo was created in this thesis. The aim of this thesis is to model the building in the Dymola/Modelica environment and calibrate it, and then apply different rule based control strategies and evaluate them.

The framework in the thesis presents up to date research about building performance simulation and its limitations. It also highlights how Modelica performs as a building performance simulation (BPS) tool and how to calibrate a modelled building. Lastly, the framework compares the impact of MPCs on modelled buildings to rule based controls (RBCs). The research indicate the potential of MPCs on the energy use in buildings and the reduction in peak load, but MPCs can be optimized to minimize different objective functions depending on the desired outcome.

The office building has eight floors and a basement, but it is only parts of the basement and the second to the seventh floor that are connected to the hydronic heating system. SINTEF conducted measurements in the physical building during the spring of 2020. These measurements are used for the calibration process, and some of the measured data are used as inputs to the modelled building to reduce the number of unknowns in the model. A weather file containing the measured weather in 2020 is created to ensure that the modelled building experiences comparable weather to the building in Oslo during the measurement period. The initial step in the calibration process is to calibrate the sixth floor of the building, as there are fewer sources of error when only one floor is considered. The nominal power of the radiators and the internal heat gains are varied in the model to obtain a calibrated model of the sixth floor. The nominal power for the West circuit is 35 W/m^2 and 25 W/m^2 for the East circuit. The internal heat gains in the models are the same as the values from Standard Norge (2020), but after the 12th of March there are no people present and the heat added by machines and lights are set to the lowest level. The model is calibrated once it is within the limits of statistical indices set by The American Society of Heating, Refrigerating and Air-Conditioning Engineers (ASHRAE). The same inputs that were used to calibrate the sixth floor of the building are then applied to the entire building. The model of the sixth floor and the modelled building are within the tolerance levels as set by ASHRAE.

Different RBC strategies are applied to the calibrated model once the modelled building

is calibrated. During the evaluation of the controls, the modelled building experiences normal operating conditions such as typical meteorological data. The three controls considered for the evaluation is a weather compensated curve (WCC) with a night setback, a WCC without a night setback and a WCC where the pumps turn off at night. The WCC is optimized for each case to ensure that the indoor air temperature is within acceptable levels for all of the cases. The case without a night setback has the highest energy use and obtains the best indoor air temperature, whereas the case where the pumps turn off at night has the lowest energy use and has the most hours below acceptable indoor air temperature levels of 19 °C.

Lastly a sensitivity analysis of the modelled building with a rule based control consisting of a WCC and a night setback is performed. It highlights that the level of blinds and internal heat gains do not impact the energy use in the building to a large degree, but assuming less blinds in the modelled building can reduce the number of hours below 19 °C in the building. Moreover, by reducing the night and weekend setback of the WCC from 10 to 15 °C the building consumes 12 % less energy. However, this significantly impacts the indoor air temperature in the building as the number of hours below 19 °C increase.

Sammendrag

Bygninger bidrar til verdens energibruk og utslipp av klimagasser. En foreslått løsning for å redusere energibruken i eksisterende bygninger er å implementere avanserte kontrollstrategier. Et forslag er modell prediktiv kontroll (MPC). Tidligere forskning på modell prediktiv kontroll har belyst potensialet denne kontrollstrategien har til å redusere energibruken ved å implementere den i eksisterende bygg. Modell prediktiv kontroll må være tilpasset bygget den skal kontrollere. Målet for oppgaven er å lage en forenklet emulator av et kontorbygg i Oslo for å kunne indeksere, sammenligne og eksperimentere på kontrollalgoritmen offline.

Rammeverket for oppgaven presenterer oppdatert forskning om bygningssimulering og dens begrensninger. Det blir også belyst hvordan Modelica opptrer som et bygningssimuleringsverktøy og hvordan man kan kalibrere et bygg. Til slutt sammenligner rammeverket effekten av modell prediktiv kontroll mot regelbasert kontroll. Forskningen indikerer at MPC-er har stort potensiale med tanke på å redusere energibruken i bygninger og å redusere toppbelastningen, men MPC-er kan også bli optimalisert til å minimere andre objektfunksjoner avhengig av hva man ønsker at MPC-en skal kontrollere.

Kontorbygget har åtte etasjer og en kjeller, men det er bare deler av kjelleren og andre til syvende etasje som er dekket av det vannbårne varmesystemet. SINTEF utførte målinger i bygget våren 2020. Disse målingene brukes for kalibreringsprosessen, og noen av de målte dataene brukes som inndata i den modellerte bygningen for å redusere antall ukjente i modellen. En værfil som inneholder værdata for 2020 er laget for å påse at den modellerte bygningen opplever det samme været som bygget hadde da målingene ble utført. Det første steget i kalibreringsprosessen er å kalibrere sjette etasje av bygget, ettersom det er færre feilkilder når man kun undersøker én etasje. Den nominelle effekten til radiatorene og varmebidraget fra personer, lys og utstyr er variert for å kalibrere modellen av sjette etasjen. Den nominelle effekten for vestkretsen er 35 W/m^2 og for østkretsen er det 25 W/m^2 for det vannbårne systemet. Varmetilførselen fra personer, lys og maskiner er satt til det samme som verdiene fra Standard Norge (2020), men etter 12. mars 2020 er varmeeffekten fra mennesker satt til 0 og maskiner og lys er satt til det laveste nivået. Modellen skal være kalibrert når den er innenfor grensene til de statistiske indeksene satt av ASHRAE. De samme inndataene som ble brukt for å kalibrere sjetteetasjen er brukt for å kalibrere hele bygget.

Når modellen er kalibrert, er forskjellige regelbaserte kontroller testet på den kalibrert modellen. Under evalueringsprosessen brukes typiske værdata i modellen. De tre kontrollene som evalueres er en som har utekompenseringskurve med nattsenking, en som har utekompenseringskurve uten nattsenking og en siste kontroll som har utekompenseringskurve hvor pumpene skrus av på natten og i helgene. Utekompenseringskurven er optimalisert til hver kontroll for å oppnå innetemperatur i sonene innenfor akseptable nivåer.

Kontrollen som har utekompenseringskurve uten nattsenking har høyest energibruk og har best innetemperatur gjennom året, mens kontrollen hvor pumpene skurs av på nettene og i helgene har lavest energibruk og flest timer utenfor akseptabel innetemperatur på 19 °C.

Til slutt er det gjennomført en sensitivitetsanalyse av det modellerte bygget som har en regelbasert kontroll med utekompenseringskurve og nattsenking. Denne analysen belyser at solskjerming og varmeeffekten fra folk, lys og utstyr ikke påvirker energibruken i bygget til en stor grad, men mindre solskjerming i det modellerte bygget kan redusere antall timer under 19 °C med denne kontrollstrategien. Å endre nattsenkingen på utekompenseringskurven fra 10 til 15 °C fører til at bygget bruker 12 % mindre energi. Derimot øker dette antallet timer i arbeidstiden under 19 °C i bygget.

Preface

This Master's thesis represents the final work of my five years at the Norwegian University of Science and Technology. It finalizes my schooling at NTNU and has been the most challenging and rewarding experience of my life. The work is conducted at the Department of Energy and Process Engineering and supported by researchers at SINTEF Community in Oslo. It is written for readers familiar with building performance simulation who should have no trouble following the content of the thesis.

Throughout my time at NTNU, I have been introduced to new people whose friendship I will always cherish. I also appreciate the knowledge and the character-building that NTNU has imparted to me after these memorable five years.

Moreover, I would like to thank my supervisors, Laurent Georges, Harald Taxt Walnum and Igor Sartori, for guiding me in the right direction and patiently helping me during this work. Thank you also to Marius Bagle. And lastly, I would like to thank my family and friends, particularly Goran, for supporting me during the five years at NTNU.

Martine Walvik Gundersen

Table of Contents

List of Tables

List of Figures

Abbreviations

ACH	=	Air Changes per Hour
ACS	=	Advanced Control Strategies
AHU	=	Air Handling Unit
BIM	=	Building Information Modeling
BPS	=	Building Performance Simulation
CAD	=	Computer Aided Design
CAV	=	Constant Air Volume
CFD	=	Computational Fluid Dynamics
CV(RMSE)	=	Coefficient of Variation of the Root Mean Square Error
DHI	=	Diffuse Horizontal Irradiance
DNI	=	Direct Normal Irradiance
GHI	=	Global Horizontal Irradiance
HVAC	=	Heating, Ventilation and Air Conditioning
MBE	=	Mean Bias Error
MPC	=	Model Predictive Control
RBC	=	Rule Based Control
SPA	=	Solar Position Algorithm
TEASER	=	Tool for Energy Analysis and Simulation for Efficient Retrofit
TMY	=	Typical Meteorological Year
WCC	=	Weather Compensated Curve

Chapter 1

Introduction

The European Commission (2020) states that buildings contribute to more than 40% of the European Union's energy consumption and 36% of the European Union's greenhouse gas emissions. The European Parliament (2010) therefore created the energy performance of buildings directive to promote policies that will ensure more energy efficient buildings by 2050 as well as giving consumers and businesses the possibility of making more informed choices. Afram and Janabi-Sharifi (2014) further highlight that the building services and heating, ventilation and air conditioning systems contribute up to 50 % of the energy use in buildings. One measure that the EU promotes to reduce the energy use in buildings in the future is smart technology, through requirements such as control and automation of buildings and devices that control the room temperature. Advanced control strategies (ACSs), such as Model Predictive Control (MPC), have proven to be an option in reducing the energy consumption by HVAC systems in buildings.

Drgoňa et al. (2020) state that MPC is a real-time control of a model of the building that aims to minimize an objective function. MPCs are flexible in that their objective functions can target several different parameters, for example, the objective function can be the minimization of energy use or the maximization of thermal comfort. For the Master's thesis, the impact of MPCs on minimizing the energy use in buildings is the main focus. Afram and Janabi-Sharifi (2014) argue that even the most basic form of MPC, which has linear constraints and simple disturbances, outperforms the conventional controls. One such example is from a study by Prívara et al. (2011) which found that the MPC maintained the thermal comfort of a large university building whilst using 29 % less energy compared to weather compensated controller which also included a weather forecast in its control. Walnum et al. (2020) also showed that MPC reduces the energy consumption by 12 % compared to a weather compensation curve, although this simulation is during rather idealized conditions.

The risk of malfunction and the investment costs of applying an ACS to existing buildings were highlighted by Blum et al. (2019) as barriers to adapting such strategies to reduce

the energy consumption in buildings. A solution to overcome these issues is to test the strategies in a simulation that uses an accurate model of the actual building. An emulator that includes a detailed model of the building and its heating system should be accurate enough to represent the controlled building in this case.

The main purpose of this Master's thesis is to develop a model of SINTEF's office building in Oslo to be used as an emulator to compare control algorithms for MPCs. A model of the building must include its thermal dynamics, in order for the MPC to handle changes to the thermal mass in the building. There are measurement data from the building, such as temperature and flow levels of the radiator and ventilation circuits as well as the indoor air temperature. These measurements are used to calibrate the model.

The thesis has two main parts. The first is to develop a model of the test building which uses input data from the measurements conducted in the spring of 2020, and ensure that this model is calibrated. The second part of the thesis is to apply different rule based control strategies (RBCs) to the calibrated model and evaluate their impact on the building's energy use and indoor air temperature.

1.1 Scope of the Master's Thesis

The specialization project conducted during the fall of 2020 focused on developing a first version of a simplified model of the building. The specialization project modelled the sixth floor of SINTEF's building in IDA ICE and Modelica and compared the results of the two building performance simulation (BPS) tools. The Master's thesis will continue to expand on the findings from the specialization project. There are four goals of the Master's thesis.

1. Develop an improved version of the model (from the project work). The version should have an updated space-heating system, a ventilation system, a model of the connection to the district heating grid and the model should be separated into multiple zones.
2. Update the schedule for the internal heat gains and the blinds in the model.
3. Validate and calibrate the model against existing measurements.
4. Evaluate control strategies for the building using the validated model.

The refinement to the scope of the Master's thesis is done in agreement with the supervisors. Goals two and three will use input values from the physical building. The final goal investigates how the modelled building performs under typical meteorological year (TMY) weather and rule based controls in the building.

1.2 Overview of the Master's Thesis

The introduction highlights the motivation for this Master's thesis. Chapter 2 goes into detail about the framework of the thesis, by investigating the use and limitations of building performance simulations tools in relevant literature and the theory behind the model in the Master's thesis. Chapter 3 presents the method to develop the modelled building, and highlights the assumptions and simplifications that are used in the model. Chapter 4 describes the calibration process and obtains the inputs to be used in the modelled building. It also includes an analysis of the calibration process. Chapter 5 presents the control strategies to be applied in the modelled building and the results of the building simulations during normal operation are presented and analysed in more detail. Lastly, the conclusion from the Master's thesis is drawn in chapter 6.

Use of the Specialization Project from December 2020

The specialization project was the introductory work for the Master's thesis. The title of the project was "Modelica Emulator for MPC Applications in Buildings". The specialization project by Gundersen (2020) was the author's own work. Therefore, some of the paragraphs from the specialization work will be reused in the Master's thesis. The introduction and a significant portion of the framework, namely Chapters 2.1 - 2.1.2, 2.2-2.5.3 and the methodology in Chapter 3 are modified chapters of the text in the specialization project.

Chapter 2

Framework

In order to understand how an emulator can benefit the process of making existing buildings more energy efficient by means of more optimized control, it is important to understand how building performance simulation works and its limitations. Moreover, in this chapter the simplifications and assumptions in building performance simulation tools are highlighted to create the framework for understanding the underlying principles in the model.

2.1 Building Performance Simulation

Hensen and Lamberts (2011) suggest that in order to achieve the goals that are set for buildings in terms of energy consumption and emissions, one needs to opt for computational building performance simulation. Traditional engineering design tools are static and try to provide an exact solution to a simplified model of a fraction of reality. BPS "is multi-disciplinary, problem-oriented and wide(r) in scope. It assumes dynamic (and continuous in time) boundary conditions, and is normally based on numerical methods that aim to provide an approximate solution of a realistic model of complexity in the real world" (Hensen and Lamberts, 2011, Page 3).

There are several methods of modelling buildings. Hensen and Lamberts (2011) explain three of them, white-box, black-box and grey-box. White-box modelling (often called first principle models) involves capturing the entire model and making use of physical laws to create a model of the building, and it is not based on experimental data. This is computationally expensive and it is difficult to provide the level of detail required to get an accurate model. Black-box modelling (also called empirical models) is to rely on experimental data to model the building and there is no need to know the physics in the building as the model continuously gets feedback from the data. However, this model can only operate within the domain of its experimental data. A grey-box model (quasi-first principle model) is somewhere in between white and black box modelling and often relies on a network analogy (R-C circuit) to operate, according to Serale et al. (2018). Moreover, the

distinction between grey-box and a white-box modelling is that the grey-box model needs some empirical input. It is also distinguished from pure empirical models, since empirical models result from curve-fitting of measurements (Hensen and Lamberts, 2011, Page 318). Therefore, as long as the model does not solely rely on prior physical knowledge of the system, it is grey-box modelling. By using the aforementioned definitions, it is evident that the model for this project is a grey box model.

2.1.1 Building Simulation and The Performance Gap

The building models are only a representation of reality, and there will therefore be a difference between the models and the actual buildings. The performance gap in this case is the energy difference of an entire building between the prediction and the measurement stages. de Wilde (2014) argues that the causes for the gap can be grouped into categories, related to the design, construction and operational stages. In the design stage, future problems can arise as the design team cannot predict the future use of the building, oversizing HVAC components and the thermal concept might be poor. Moreover, appropriate use of BPS tools to ensure optimal design is key, but also a correct analysis of the results. Yet, the analyst cannot easily predict the future, so the design will nonetheless be subject to uncertainties. In the construction stage, deviations from the original design might occur where the quality of the building is not in accordance with the original design. In the final stage, operational, the performance gap is in most cases due to a different occupant schedule than the assumptions in the design phase. de Wilde (2014) developed a framework for further investigation into the performance gap, with a hope to help bridge the gap. The author investigated a pilot study of a nine-floor office building in Plymouth. The performance gap between the measured and simulated values shows that it varies from month to month, when it comes to the gas and electricity use. Gas use was predicted by an error of 5 % whereas the error in the electricity consumption was in the order of 30 %. When investigating the measured energy use over 2011 and 2012 and comparing that to the simulated values, it is clear that in the colder years the performance gap will be wider than in the warmer years. The article follows up with a framework of issues that needs to be addressed when investigating the performance gap. This framework includes, among other points, validation and verification for the prediction model and that the input data used for predictions need to be improved.

Moreover, the performance gap is also present in private households. Jones et al. (2015) investigated the performance gap by completing a case study of six identical flats during the first year of occupation. The flats are in Torquay in the United Kingdom (UK). They are designed to be ”low energy” or ”high performance” houses, and the area of each flat is 80,5 m^2. The buildings were modelled in DesignBuilder, the original predicted values for expected performance of the flats were collected from the architectural design team and the measured values were obtained by installing an automated monitoring system in each of the flats. The results show that the predicted and modelled consumption of gas were overpredicted by a factor of 1,7 and 1,5, respectively, when compared to the measured mean annual gas consumption. However, the predicted and modelled electricity consumption were underpredicted by a factor of 0,5 and 0,8, respectively, compared to the measured mean annual electricity consumption.

Uncertainties about the future can make the buildings perform worse than expected over their lifetime compared to the expected performance as observed during the design phase. Kotireddy et al. (2019) investigated different approaches to mitigating the uncertainties that are present when developing models of buildings, such as the future climate or the occupant behaviour. Such uncertainties are the reason for the performance gap between modelled and actual performance for a building. The results show that scenario analysis can be used when the the future uncertainties are unknown. This result was demonstrated by investigating a residential building case study, with different stakeholders. The building performance robustness was investigated by looking at energy consumption, CO_2 emissions and financial indicators. A conservative approach was the max-min approach, and a less conservative approach was the minimax regret since this one was close to optimal performance for each scenario. The best-case and worst-case method is preferred when the building has to deliver the best results even during the worst conditions. The results of this study illustrate the need to design robust buildings in order to reduce the performance gap.

2.1.2 The Limitations of Building Simulation

It is important to understand the limitations of BPS tools in order to explain why there are discrepancies between the buildings and the modelled buildings and how to mitigate them as much as possible. Solmaz (2019) investigated and compared BPS tools. The comparisons show that most of the simulation tools are used in the later design stages, and their use in early design and retrofit stages is limited. The author argues that the use of BPS tools in operation, management and retrofit of existing buildings should be improved. Moreover the results show that it is beneficial for the user of such tools to have an understanding about building physics, environmental systems or Computer Aided Design (CAD)/Building Information Modelling (BIM) systems in order to understand the simulation process and results properly. The article further summarizes some limitations to BPS tools, such as the interoperability issues with data exchange between BIM/CAD programs and simulation tools that are yet to be solved and that it is crucial for BPS tools of the future to be able to model building stocks and simulate on an urban scale to ensure that energy and environmental goals at regional/national level are reached.

Researchers claim that building simulation tools are important in order to optimize the buildings' impact on the environment and Mahdavi (2020) discussed this claim. He argues that building performance simulation tools are a great asset to the design of a building, given that a reliable method is employed by people who know its limitations. Furthermore, the building industry does impact the global environment negatively, but reducing its impact is not nearly as efficient in mitigating environmental issues as strategies related to reducing the impact due to, for instance, population growth. Moreover, Williamson (2010) wished to illuminate that it is crucial to consider more than the quantitative accuracy of building performance simulation. He argues that when considering if the information in the simulation is good, one should consider what information is presented (knowledge), and also the information that is missing (ignorance). Moreover, the author argues that credibility relates to the simulation means, but also to the use of simulation results. The author highlights this point by illustrating that compliance to the Building Code of Aus-

tralia can be demonstrated by achieving a Star Rating, based on the simulated results for green house gas emissions of new buildings. However he shows that there is no significant correlation between the Star Rating and actual greenhouse gas emissions. The article also highlights that the dependability of building simulation is not considered in many BPS tools, as changing conditions in the future are difficult to predict but will definitely play a significant role in the energy use in buildings. Lastly, the author highlights the problem of confirmability in BPS where a study consistently found differences of $\pm$ 50 % in total building energy consumption when different operators were asked to simulate the same building and using the same software. The author concludes by stating that simulations should be viewed as incomplete perspectives of a problem that forms a basis for humans to make wise judgements.

2.1.3 Calibration

The Master's thesis aims to calibrate the model to measurements from the building. Calibration is to tune parameters in a BPS model in order for the simulation results to be more in line with the measured values from the actual building. Reddy (2006) states that there are two reasons for calibrating models. The first reason is to identify the energy saving potential in the building and the second reason is that calibration adds more confidence in the monitoring of the building once the energy saving measures are implemented. Reddy (2006) recommends to perform a sensitivity analysis prior to starting the calibration process in order to identify which parameters are worthwhile to calibrate. The author also include the uncertainty limits by The American Society of Heating, Refrigerating and Air-Conditioning Engineers (2014) (ASHRAE) for calibrated simulations (Coefficient of Variation of the Root Mean Square Error (CV(RMSE)) of $\pm 30\%$ when using hourly data) and comments that ASHRAE has not specified why these limits were proposed. It should be noted that there is no standard threshold for model calibration for demand response using thermal mass applications. Reddy (2006) assumes that the tolerance intervals were set due to the experience of the modellers that performed the calibrations.

Ascione et al. (2020) investigated an existing building in the South of Italy in order to optimize an energy retrofit as the building had a high energy consumption. They installed sensors in the building to obtain data and used the measured data to calibrate the model. The authors refer, like Reddy (2006), to the thresholds presented by ASHRAE. ASHRAE highlights that the CV(RMSE) should be calculated for the energy consumption in the building. However, Ascione et al. (2020) state that the measured energy consumption of their industrial building also included the energy use by the production lines. Therefore, the authors decided to compare trends in the simulated and measured indoor temperatures. Following the implementation of the model according to Italian standards, the authors calibrate the building model by observing the discrepancy between the heating schedules in the standards and the observed data from the building. By changing the heating schedules, the simulated data are within acceptable thresholds as presented by ASHRAE. Ascione et al. (2020) conclude, for the calibration part, that as long as the error indicators (Mean Bias Error (MBE) and CV(RMSE)) are within acceptable levels, the model is appropriately calibrated.

Moreover, Royapoor and Roskilly (2015) aspired to calibrate a five storey building in the UK by creating a model of the building in EnergyPlus. The authors highlight that there are two main sources of error present when comparing measured and simulated data: measurement error and model error. Measurement error is error due to the equipment used when measuring the building. Model error relates to uncertainty due to sources related to specification, modelling and scenario. Specification is for instance an inaccurate description of the building's systems or construction, whereas modelling related sources of uncertainty are due to simplifications in the model compared to reality. Scenario related sources of uncertainty occur because internal or external parameters are different to reality. Royapoor and Roskilly (2015) underline that the occupant behaviour (internal uncertainty) is one of the most prominent sources of error in model predictions. The author's final calibrated model had a deviation of 1,08 % to the annual electricity consumption of the model. Royapoor and Roskilly (2015) also presented the hourly deviations in MBE and CV(RMSE) indices on a monthly basis and found the largest deviations in December. The authors also concluded that the model had a more accurate temperature prediction whenever the Air Handling Unit (AHU) was idle, which confirmed their initial assumption that the HVAC category has the largest magnitude of error.

2.2 Modelica as a Building Performance Simulation Tool

The Master's thesis will use the Dymola/Modelica environment to create the model of the building in Oslo. Modelica is an equation-based modelling language. The libraries for buildings were created in response to the previous era of building simulation which used imperative programming languages. Imperative languages (such as C or C++) often cause the procedure of the numerical solution to be part of the actual model equations according to Wetter et al. (2016). Moreover, Modelica is an open-source language. There are several libraries available in Modelica to model buildings, and currently there are four libraries that are open source: AixLib, BuildingSystems, Buildings and IDEAS. However, from 2012 to 2017 the International Energy Agency (IEA) initiated a project called the "Annex 60 Modelica Library". Wetter et al. (2015) state that the purpose of the project was to create a common library that is at the core of the previously mentioned libraries. Thus it is now possible to combine several libraries, since the base classes are the same, or one can further develop the components in the specific libraries. It is decided to model the building in Modelica for this project work as this environment allows simulation of buildings using external control, such as MPC.

Since Modelica was created in 1998, the use of it in industrial sectors and in demanding computations is significant (Hensen and Lamberts, 2011, Page 389). However, the authors also state that Modelica for BPS was rarely used at the time of writing. The use of Modelica as a BPS tool has increased after this. One reason is the way Modelica differs from traditional BPS tools in modelling HVAC components. Modelica allows to explicitly alter model equations and the solver is independent from the model definition according to Drgoňa et al. (2020). Another reason is the ability to export Functional Mock-up Units (FMUs) which can be used for co-simulation between Modelica and Python. Blum et al. (2019) developed the BOPTEST framework to test advanced control strategies through

simulation before implementing them in buildings. BOPTEST stands for Building Optimization Performance Test and it uses the Functional Mockup Interface (FMI) and Modelica to simulate different buildings' response to various control strategies. The identification of different KPIs for the model and values for stakeholders in the paper by Blum et al. (2019) illustrate the potential of Modelica to aid and benefit building managers and other stakeholders.

Bontemps and Mora (2015) created a model of a building located close to Munich, Germany, and compared the simulation results to measurements conducted in the building. The building was a a three floor building, but the model was only concerned with the ground floor. The model of the building in the case study is modelled using the Buildings library in Modelica. During the measurements, they had different scenarios where on some days they had a constant set temperature, some days there was a free-float period and a Randomly Ordered Logarithmic Binary Sequence to ensure no correlation between solar and heat inputs. They observed that the residual between the measured and the simulated temperature was no more than 5 °C, when there was a set temperature. It was also observed that in some of the zones the simulated temperature decreased faster than the measured temperature when the heating was stopped, where the discrepancy was almost constant during the free-float periods. They also observed that there was a discrepancy in the heating power in the various zones between the measured and simulated values. The authors explain these differences due to modelling and measurement errors, and emphasize that further research is required to achieve an empirical model validation.

Jorissen et al. (2019) wanted to prove that Modelica can be used for complex buildings, and that an integrated model with multiple zones and its envelope, HVAC system and controls could be modeled in a single model. They verified and calibrated a 32-zone model in Modelica with measured data. It was proven that HVAC models are accurate, meaning an order of error of a few percentages, whereas the zone dynamics had a deviation of around 2 K. Due to the nature of the actual building, which had a concrete core activation system, the error in cooling and heating provided by said systems were under predicted. They still argue that the findings can be used for design and control, but less for absolute energy savings.

Wetter et al. (2016) wanted to illustrate the reduction in computing time by using equation-based languages compared to "conventional building simulation programs". The authors created a net zero energy neighbourhood in Modelica using the Buildings library. They then wanted to compare the use of collocation-based optimization method to the simulation-based method to solve a constrained nonlinear optimal control problem. In equation-based languages, the collocation-based method is used and in "conventional building simulation programs" the simulation-based method is used. The comparison of the two methods illustrated that the total computing time in for the collocation-based optimization method was 7,75 seconds, whereas the total computing time for the simulation-based optimization method was 17401 seconds. The equation-based languages thus solve the problem 2200 times faster than the simulation-based method, even though the equation-based languages also had a larger optimization problem to solve.

Lastly, González and Yebra (2015) compared Modelica to DesignBuilder. DesignBuilder is a special purpose building simulation tool, whereas Modelica is an object-oriented modeling language. The authors wanted to compare the results of a specialized building simulation tool (DesignBuilder), to that of a general purpose tool (Modelica). The building they modelled is a simplified building, a cube with a length of 7 m, depth of 4,6 m and a height of 3 m. The building is located in Granada in Spain. The results show a maximum total error of 0,69 % in the simulation of a complete day, when investigating the inside air temperature and also a maximum difference of inside air temperature of 2 °C between the two models in the month of June. They argue that the difference between them is due to the modelling hypothesis used in the implementation of the models. The authors conclude that Modelica is a good option for dynamic modelling of buildings when compared to specialized tools.

2.3 The Modelled Zone

Within the Modelica environment, there are two main methods of modelling a zone - the detailed or the reduced order method. It is decided to use the reduced order method as this has less spatial discretization in each element which makes it more ideal for simulating multiple buildings or for model predictive control, according to Lawrence Berkeley National Laboratory (2020). Within the reduced order method, the Reduced Order Models (ROM) will be used. The ROMs rely on the RC analogy. The RC analogy is the idea that thermal elements can be modelled as thermal networks with thermal resistances and capacities to illustrate heat storage and transfer. The thermal zone with four elements is illustrated in Figure 2.1 and one observes that it contains elements for the exterior and interior walls, the floor and the roof.

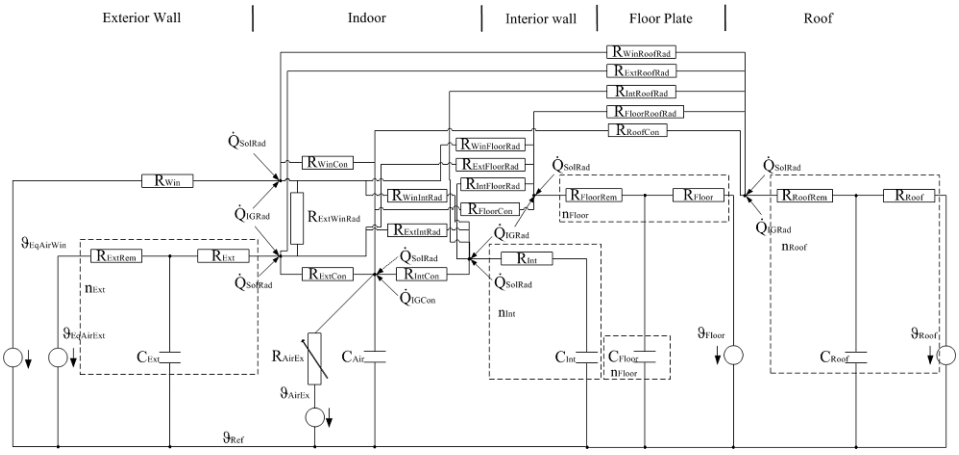

Figure 2.1: The thermal zone with four elements, created by Lawrence Berkeley National Laboratory (2020).

2.3.1 TEASER

The reduced order thermal zone model in the Buildings library within the Modelica environment requires explicit values for the resistances and capacities for the elements in the zone. As this is difficult to obtain and calculate correctly, TEASER (Tool for Energy Analysis and Simulation for Efficient Retrofit) is used to create the thermal zone. TEASER is a software that allows for fast implementation of zone elements, based on different saved libraries of building elements and their physical properties which was created by RWTH Aachen University (2017). By identifying the building elements of the zone and their measurements, one can use the predefined values from TEASER's libraries which then calculates the required explicit values for inputs such as capacities and resistances.

2.3.2 Standard Room Model

The air within a building is driven by for instance pressure differences, stack effects, HVAC components and people. There are various ways to model this within BPS tools, ranging from very detailed to assumptions of perfectly mixed air. The standard room model is used for this model. Yu et al. (2019) state that the standard room model or multi-zone models regard the room or zone as whole, where density, pressure and temperature are assumed to be homogeneous. They assume therefore that the temperature and pollution are evenly distributed in the zone. The benefits are the low computational time and the easy implementation. However, the accuracy is not as good as the other models and with the increasing capabilities of computers, it should be possible to improve the accuracy of models compared to actual zones. Georges et al. (2019) also highlight that airflows within zones are not captured using this method, which causes inaccurate simulation results when considering local thermal comfort.

2.3.3 Internal Masses

In a building, different elements influence the heat transfer between the inside and the outside of the zone, as well as heat exchange within the zone. Hicham and Heiselberg (2017) investigated the influence of internal mass on the thermal dynamics of a building. Many people and programs modelling buildings simply assume that the zones are not furnished or do not take into account the impact from the internal walls or doors. The authors found that indoor thermal masses can account for up to 40 % of the total hourly heat capacity in the room, and that it can increase the building time constant of many hours.

2.4 Radiation Exchange with the Outdoors

In order to consider the solar radiation hitting the exterior surfaces, one can either consider the heat load hitting the exterior surface or add a correction term to the outdoor air temperature to get the equivalent air temperature. The ROM in Modelica uses the latter. Lauster et al. (2014) showed that by substituting the outdoor air temperature with an equivalent air temperature, one can incorporate the long-wave radiation (such as from the sun) into the

model. The authors compared the simulation times and accuracy between several cases, but for the purpose of the model in this project it is interesting to investigate the difference between the model using a heat balance and the model using equivalent air temperature, as described in the German Guideline VDI 6007.

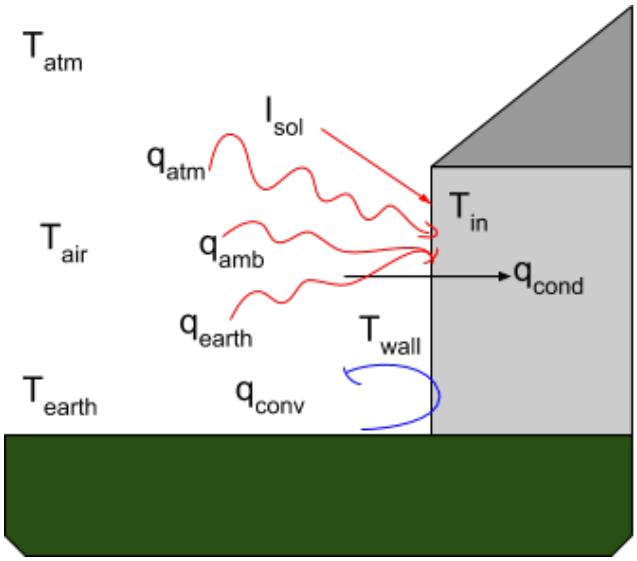

Figure 2.2: Heat flows on outer walls. Adopted from Lauster et al. (2014).

In Figure 2.2 one can observe the heat flows on the outer walls of a building. Long-wave radiation is rarely available in the measurement data compared to short-wave radiation. Moreover, long-wave radiation is further divided into atmospheric, ambient and partly reflected ground radiation and then empirical methods are used to consider long-wave radiation as a function of outdoor temperature and cloud coverage. The overall heat balance is presented in Equation 2.1.

$$q_{cond} = q_{short-wave} + q_{long-wave} + q_{conv} \tag{2.1}$$

Both models assume the outdoor wall to be adiabatic, as a first simplification, meaning $q_{cond} = 0$.

The equivalent air temperature model according to VDI 6007 simplifies the heat flows to one equivalent heat flux, as seen in Equation 2.2.

$$\alpha_{comb} \cdot (T_{eq} - T_{wall}) = q_{short-wave} + q_{long-wave} + q_{conv} \tag{2.2}$$

Here a combined radiative and convective coefficient of heat transfer is introduced, α_{comb}. This model linearizes the long-wave radiation, by expressing T_{atm} and T_{earth} as long-wave radiation heat flows.

$$T_{atm} = \left(\frac{E_{atm}}{\epsilon_{earth} \cdot \sigma} \right)^{0,25} \tag{2.3a}$$

$$T_{earth} = \left(\frac{E_{earth}}{\epsilon_{earth} \cdot \sigma} \right)^{0,25} \tag{2.3b}$$

$$\alpha_{rad} = \frac{T_{atm}^4 - T_{earth}^4}{(T_{atm} - T_{earth})} \cdot \sigma \cdot \epsilon_{wall} \tag{2.3c}$$

Using the simplifications mentioned in Equation 2.3, one can solve the heat balance as presented in Equation 2.2. This gives Equation 2.4.

$$\begin{aligned} \alpha_{comb} \cdot (T_{eq} - T_{wall}) = \alpha_{rad} \cdot ((T_{atm} - T_{air}) \cdot \varphi_{atm} \\ + (T_{earth} - T_{air}) \cdot \varphi_{earth})) + q_{short-wave} \end{aligned} \tag{2.4}$$

φ_{atm} and φ_{earth} are the view factors of the long wave radiation source of the atmosphere and the earth respectively. The simplification of the equivalent air temperature improved the simulation speed and had an acceptable accuracy when compared to a total heat balance, according to Lauster et al. (2014).

2.5 Control

There are many methods to control components within a building. Previously it was common to use RBC, but over the years the development of the MPCs have improved said controls making them a valuable asset in optimizing, for instance, energy use in buildings.

2.5.1 Rule Based Control

An RBC follows predetermined rules based on current measurements to control the component. Indoor air temperature can be one such measure. An example of RBC is the Weather Compensated Control (WCC). WCC regulates the temperature of the circulating water in the hydronic heating system depending on the outdoor temperature. The WCC is an open-loop control, meaning that the control is done without feedback. Each of the radiator circuits has an individual outdoor temperature sensor, regulating the temperature in that particular circuit.

2.5.2 Model Predictive Control

MPC has been used in multiple settings throughout the history. This is particularly evident during the last decade, as the computational power of building systems has increased. Drgoňa et al. (2020) state that MPC is a real-time control of a model of the building that aims to minimize an objective function. The objective function can consider for instance energy use, weather forecasts and thermal comfort. It is vital to track the trajectory of the MPC, and the goal is to ensure that the trajectory is within the acceptable levels of

a predefined and expected trajectory, as stated by Serale et al. (2018). In Figure 2.3 one observes how the prediction horizon shifts forward as the information about the plant is sampled at the current time step. The model optimizes the plant operation to the current time step.

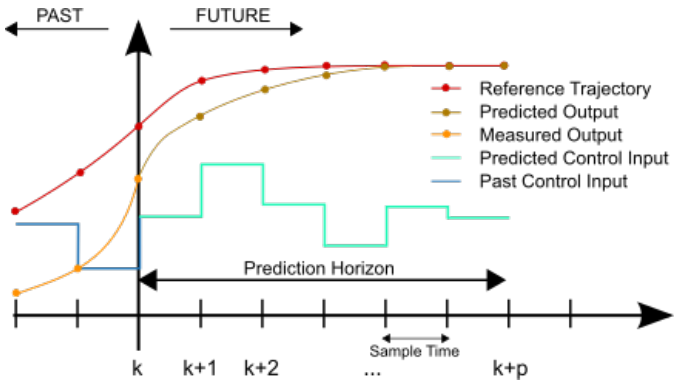

Figure 2.3: Overview of the receding horizon principle. Figure by Behrendt (2009).

2.5.3 Model Predictive Control in Building Simulation

Hensen and Lamberts (2011) state that Modelica should not be developed to replace existing specialized BPS tools, but could be a resource to develop the analysis of controls and the use of models during operation for instance. One such suggestion is the use of MPC. Drgoňa et al. (2020) reviewed papers investigating MPC for buildings. The authors aim to present an overview of MPC in buildings, which they hope can aid the implementation of advanced control strategies in buildings. Drgoňa et al. (2020) highlight the method to formulate the MPC, which methods can be used to solve the MPC and how to implement MPCs in buildings in practice. This idea is further illustrated by Serale et al. (2018). They studied 161 papers on how MPC can be used for energy management in buildings. The results show that MPC led to reductions in peak loads of around 30 % and energy savings of around 15-20 %, compared to the base case, which was a model without MPC. They argue that modern commercial, institutional and educational buildings satisfy the requirements needed to justify an investment in MPC, as the cost reduction potential the technology provides outweigh the needed investment cost. The results are reaffirmed in a study by Kavgic et al. (2015). They identified which building characteristics that are beneficial for MPC strategies, based on prototypical building energy models from North America. They argue that a high thermal mass/thermal storage is essential as it allows for instance for load shifting and pre-heating/cooling resulting in less demand for power from HVAC equipment. Moreover, they also found that high internal and external gains, high ventilation rates, twelve hour occupancy or less, broader control set-point ranges and slow HVAC system dynamic response are important features in order to implement MPC for operating buildings. They conclude by arguing that medium and large offices and secondary schools have the desired characteristics that are beneficial to MPC.

Aste et al. (2017) argue that there is a gap between the predicted (design phase) and measured (operating phase) performance of buildings which needs to be addressed. They hypothesise a reduction in energy consumption by changing from RBC to MPC to be between 15 - 30 %. They also investigated articles where a predictive-adaptive control system which forecasts climate and the cost of energy is able to achieve a 30 % reduction in energy demand in the building by optimally managing loads. They conclude that in order to mitigate the performance gap, one could benefit from adapting a unified methodological framework which connects building performance simulation, control and data analytics. This would enable multiple feed backs to improve further projects and ensuring constant evolution in the design phase by avoiding past mistakes.

Moreover, Walnum et al. (2020) implemented an MPC in a building containing a district heating consumer substation and using the Buildings library. The substation is a modified version of the consumer substation created by Kauko et al. (2018) in the Modelica/Dymola environment. The goal was to investigate the MPC with different cost functions. The results from the scenarios consisting of different controllers or different tariffs highlight the possibility of MPC to reduce the energy use and energy cost in buildings. When substituting WCC with MPC at a constant price signal, the authours found that the model with an MPC consumed 12 % less energy and the energy cost was 12 % down too when compared to the model with a WCC. However, Walnum et al. (2020) point out that the model is ideal at this state, but the results can give an indication of the energy reduction potential of MPC to WCC.

Jorissen and Helsen (2019) modeled a terraced house from 1926 and used MPC to optimize the energy use in the building. The model is based on the IDEAS library in Modelica, and the model includes a hydronic heating system (radiators), ventilation system and the building envelope. This model has nine zones, and uses a hysteresis to control the radiators. The combined pressure drop of the thermostatic valves, pipes and radiators are merged into one constant resistance to speed up the computational time of the model. They showed that the MPC uses much lower supply water temperature causing a smoother heating profile, reflected in the energy use of the heater. The MPC resulted in a 12,8 % reduction in energy use compared to the RBC, which is not a great reduction but the poorly insulated building envelope can be an explanation of this.

2.6 Weather Data

Weather data are required in the calibration process for the model to ensure that the simulated model experiences the same weather as the physical building did during the measurement period. One of the main parameters to consider is the solar radiation. Kleissl (2013) states that the components that are vital for solar-energy resource assessment are the direct normal irradiance (DNI), diffuse horizontal irradiance (DHI) and global horizontal irradiance (GHI). Although solar-energy resource assessment is outside the scope of this master's thesis, it is necessary to compute these parameters to create the weather file needed for the calibration process in Modelica. The components of solar radiation are observed in Figure 2.4.

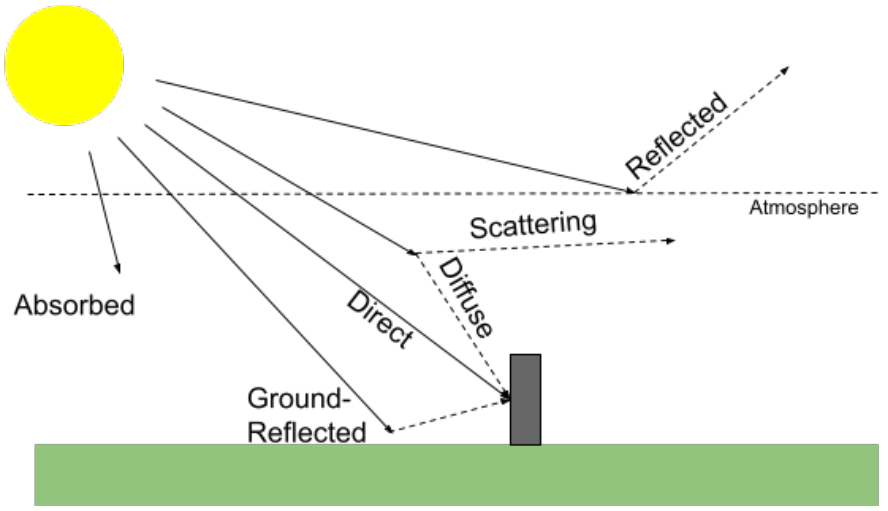

Figure 2.4: Components of solar radiation. Adopted from Rognan (2018) and Kleissl (2013).

Kleissl (2013) and Rognan (2018) state that global horizontal irradiance is the total solar radiation on a horizontal surface on earth and the direct radiation is the solar-beam radiation that is experienced by a surface normal to the sun without interference from the atmosphere. Lastly, diffuse horizontal irradiance is solar radiation that has been scattered due to for instance particles and clouds that is observed on a horizontal surface. Equation 2.5 highlights how the solar radiation components are related.

$$GHI = DNI \cdot cos(\theta_z) + DHI \tag{2.5}$$

In Equation 2.5, θ_z is the solar zenith angle. Duffie and Beckman (2013) explain that the solar zenith angle is the angle of the beam radiation on a horizontal surface. The solar zenith angle is the complement angle to the solar altitude angle. These concepts are further illustrated in Figure 2.5.

The irradiance can also be determined using Equation 2.6 which was developed by Erbs et al. (1982) to determine the DNI and DHI from GHI.

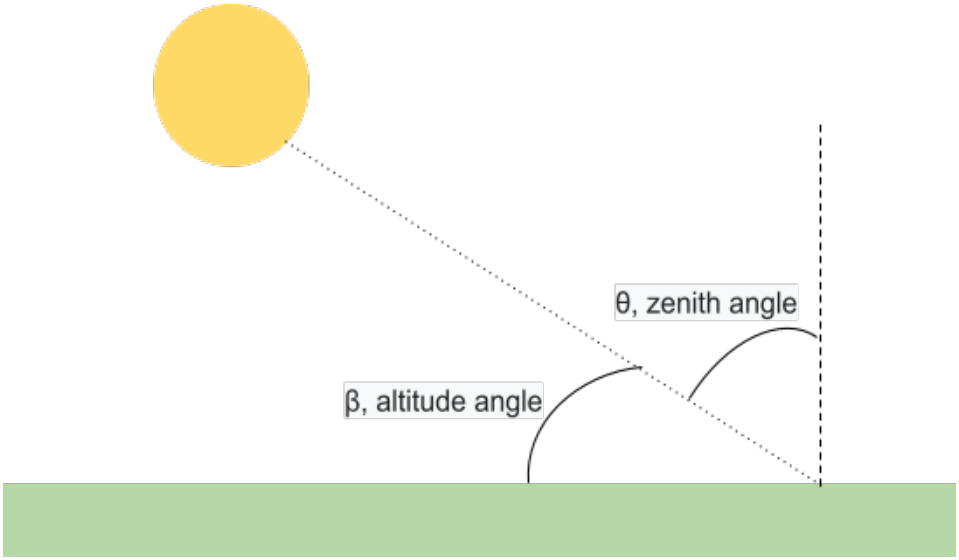

Figure 2.5: Overview of the solar zenith and altitude angles. Adopted from Duffie and Beckman (2013) and Rognan (2018).

$$DHI = DF \cdot GHI \tag{2.6}$$

DF is the diffuse fraction. Holmgren et al. (2018) state that the diffuse fraction is estimated based on empirical evidence about the relationship between the DF and k_t, where k_t is the ratio of global to extraterrestrial radiation. Following the results from Equation 2.6, one can obtain the DNI by solving Equation 2.5.

Chapter 3

Modelling the Case Building

The following section presents the process of creating the case building model in Modelica. The building is needed for calibration purposes and then to apply different rule based controls to the calibrated building to test the building during normal operations. The methodology presented in the following chapter are adaptations of sections from the author's specialization project at NTNU from the fall of 2020.

3.1 Case Building - Børrestuveien 3

The building is located in Oslo. It is an eight floor building with a basement, and an overview of the building can be seen in Figure 3.1. The total area is 3800 m^2.

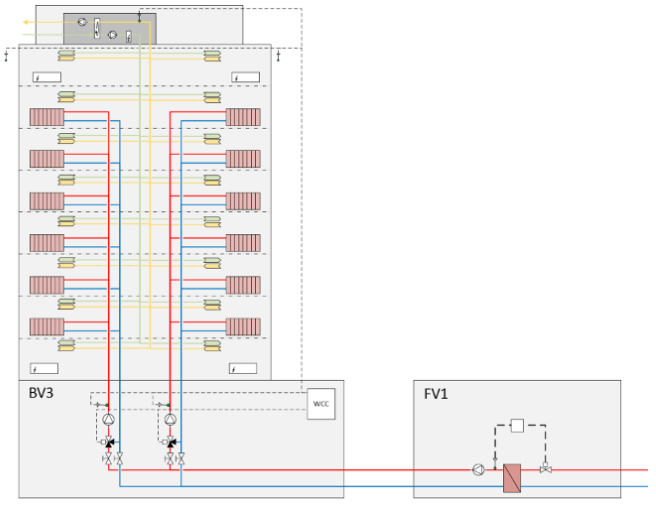

Figure 3.1: Overview of the building and its systems, as presented by Walnum (2020).

Due to Covid-19, it has not been possible to visit the case building during the period of writing the specialization project or the Master's thesis. The building has a hydronic heating system connected to the district heating grid which is split between two radiator circuits, one for the East and one for the West facade. The supply and return temperatures to the radiators follow a WCC. The basement and the second to the seventh floor are supplied by the hydronic heating system, while the remaining two floors have electric heating systems. The ventilation system consists of a rotary wheel heat recovery unit and electric reheating element. The air handling unit also follows a time schedule for when it is on and off. SINTEF performed measurements on the case building during the spring of 2020, which will form the basis for modelling the building and the calibration process.

3.2 Internal Heat Gains and Schedules

The operating schedules for the building are based on actual operating schedules and supplemented with values from Standard Norge (2020) and are presented in Figure 3.2. The ventilation schedule in Figure 3.2 is from the actual building data, and is also in line with values from Standard Norge (2020). The building is from the 1960s and it operates with a schedule for ventilation to reduce the energy consumption of the building. The load profile is when it can be assumed that the various sources are present in the zone and the proportion of the maximal heat added by each source. The ventilation system can operate either at 0%, 67% or 100% during normal operation.

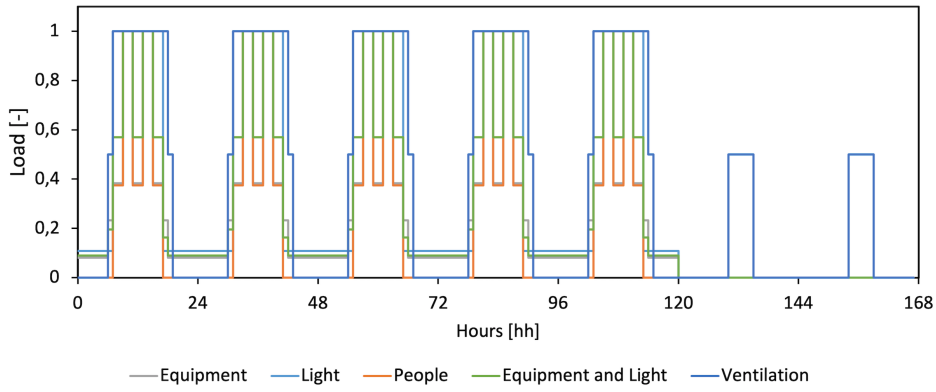

Figure 3.2: Assumed load variations throughout the week, before COVID-19.

There is no data on the number of people in the building or the heat emitted by equipment, lights and machines in the various zones. Therefore the load profiles presented in Figure 3.2 of these sources are approximated using values from Standard Norge (2020). The estimated heat added by each source from Standard Norge (2020) are then multiplied with the values in Figure 3.2 in order to become an input in Modelica. It is assumed that 50 % of the heat from people is by convection and 50 % by radiation. Lights are not added explicitly in the Modelica model, but are incorporated into the machines value.

3.3 Modelling the Building

For the specialization project, the sixth floor of the building was modelled. The Master's thesis will expand on this model by adding more floors. However, some assumptions from the specialization project are carried over into the Master's thesis such as the construction of the building, the windows and the heat exchange with the outdoors.

3.3.1 The Building Envelope

The building is a concrete construction with a brick facade. However, the different elements of the walls, floor and ceiling are not known. The regulations that were in place for the period of construction, the 1960s, will be used to obtain the U-values for the building. When the building was constructed, the guiding building regulations were from 1949. In 1969 there was a new building regulation in place. It is assumed that the building will be within the limits of the requirements of 1949, and probably closer to the values of 1969. This assumption is in line with Brattebø et al. (2014), who investigated the typology of Norwegian buildings. The different U-values are presented in Table 3.1. In the Table 3.1, the values from Brattebø et al. (2014) are the values from the apartment block in the age group 1956-1970. The assumption is that this construction is similar to the construction of the office building in Oslo.

Table 3.1: Maximum U-values [W/m^{2}K] according to Norconsult (2013) and Brattebø et al. (2014).

Element	1949	1969	Brattebø et al. (2014)
External walls	1,16	1,04	0,42
Roof over heated area	0,93	0,58	0,35
Attic floor over heated area	1,05	0,70	-
Ground floor	1,63	0,46	0,73
Windows	2,80	2,80	2,80

Building elements in the model are constructed in accordance with values and elements from Brattebø et al. (2014), Walnum (2020) and SINTEF (2015), and the materials that are unknown in the building are estimated based on the literature. The construction is presented in Table 3.2, and the values are taken from RWTH Aachen University (2017) and their library of building materials. Layer 1 is the outermost element and layer 3 is the innermost element for the components.

In Table A.1 in Appendix A, the build-up of the building elements is presented in more detail. The elements aim to have a U-value between the values presented in Table 3.1 by Brattebø et al. (2014) and the values from 1969 given by Norconsult (2013). For the external walls, the thickness of the mineral wool layer is lower (0,075 m) compared to the values in Brattebø et al. (2014) (0,1 m) in order to get the appropriate U-value. Most of the floors in the physical building have the same measurement. To model the building envelope the internal measurements of the building are used. Then the elements are expanded

Table 3.2: The build-up of building elements.

Layer	External Walls	Roof	Internal Walls	Floor
1	Brick	Concrete	Gypsum	Concrete
2	Mineral wool	Mineral wool	Mineral wool	Wood wool cement board
3	Concrete	Concrete	Gypsum	Concrete
U-value	0,428	0,362	0,569	0,572

outwards, depending on the elements that are needed to obtain the correct U-values. The building has measurements as seen in Table 3.3, although there is some uncertainty to these measurements as they were directly taken from the drawings of the floor plans with a ruler and not actual measurements. The windows are on the East and West facades and are aggregated to one large window for the model, which explains why the windows in Table 3.3 are quite long. In order to obtain measurements for the windows, the floor plan in Appendix A is used and street view photographs of the building. The height in Table 3.3 is the external height of the floor, and the internal height is 2,7 m assuming standard values from Arbeids- og sosialdepartementet (2020).

Table 3.3: Overview of the building's measurements.

Floor	Element	Direction	Length [m]	Width [m]	Height [m]
U	External Walls	East	12,57	-	3,50
	External Walls	North*	16,00	-	3,50
	External Walls	West	22,00	-	3,50
	External Walls	South	24,57	-	3,50
	Windows	South	14,57	-	1,00
	Windows	West	9,43	-	1,00
2	External Walls	East and West	27,75	-	3,50
	External Walls	North and South	9,25	-	3,50
	Internal Floor	-	27,75	9,25	-
	Internal Ceiling	-	27,75	9,25	-
	Windows	East and West	20,66	-	1,00
3-7	External Walls	East and West	30,13	-	3,50
	External Walls	North and South	10,50	-	3,50
	Internal Floor	-	30,13	10,50	-
	Internal Ceiling	-	30,13	10,50	-
	Windows	East and West	20,88	-	1,00

Table 3.3 highlights the floors included in the model and it is evident that the modelled building only considers the floors which are connected to the hydronic heating system.

U-floor has a geometry which is different to the other floors, however the area of the floor and the ceiling is 328 m^2. Moreover, the entire U-floor is greater than what is presented in Table 3.3, but the section presented in the table is the part of the floor which is heated by the hydronic heating system and is therefore the only section considered for the model. The zone supplied by the hydronic heating system in the U-floor does only have internal walls to the north, but TEASER will not allow this as a parameter. Therefore it is assumed that this is an external wall, with no windows which will give more heat loss and heat gain than an internal wall.

3.3.2 Windows

The windows from 1920 to the time period of construction were typically 1-layer glass windows, according to the numbers from Norconsult (2013). However, SINTEF (2016) states that 1-layer windows were common only until the 1930s. Both SINTEF (2016) and Brattebø et al. (2014) suggest a 2-layer insulating glass which is filled with air which will be used for the model. To find numbers for this, it is decided to use the Pilkington Optifloat Clear from Pilkington Floatglas AB (2017). This window is a clear float glass. The U-value of 2,8 W/m^2K is in accordance with the numbers from Table 3.1, the heat gain value (g) is 0,79 and the transmittance is 0,82. Lastly, there are no other openings added to the model.

3.3.3 Shading Control of Windows

The building has no controlled shading, but the blinds can be lowered manually by the people in the building to avoid glare or overheating of the building. Standard Norge (2020) states that 2 layer energy glass for windows with a U-value of 2,8 W/m^2K has a total sun factor, g_t, of 0,11 for exterior blinds. Rewriting this gives g_{blinds} of 0,15. 0,15 is multiplied with the heat value gain (g) presented in section 3.3.2 to obtain a g which includes the influence of the blinds. It is assumed that approximately 50% of the blinds are down, which is also factored into the total g. The assumption is from a photograph taken of the building in May 2020.

3.3.4 Indoor-outdoor Heat Exchange

As mentioned in Chapter 2.4, heat exchange will occur between the indoors and the outdoors. The equivalent air temperature method is used to account for the radiation exchange between the building envelope and the outdoors for the Modelica model, as mentioned in Chapter 2.4. Moreover, in the model it is decided to use a value of 5 W/m^2K for the coefficient of heat transfer for linearized radiation exchange between walls. This value is from the German Guideline VDI 6007, and was also verified in the study by Lauster et al. (2014). Lastly, the heat transfer due to internal convection is 7,7 W/m^2K (Zijdemans, 2012, p. 8).

3.3.5 Overview of the Building in Modelica

The complete overview of the modelled building is presented in Figure 3.3. The model of the building uses classes already created in Modelica, and the parameters in the classes are changed to fit the case building mentioned in Chapter 3.1.

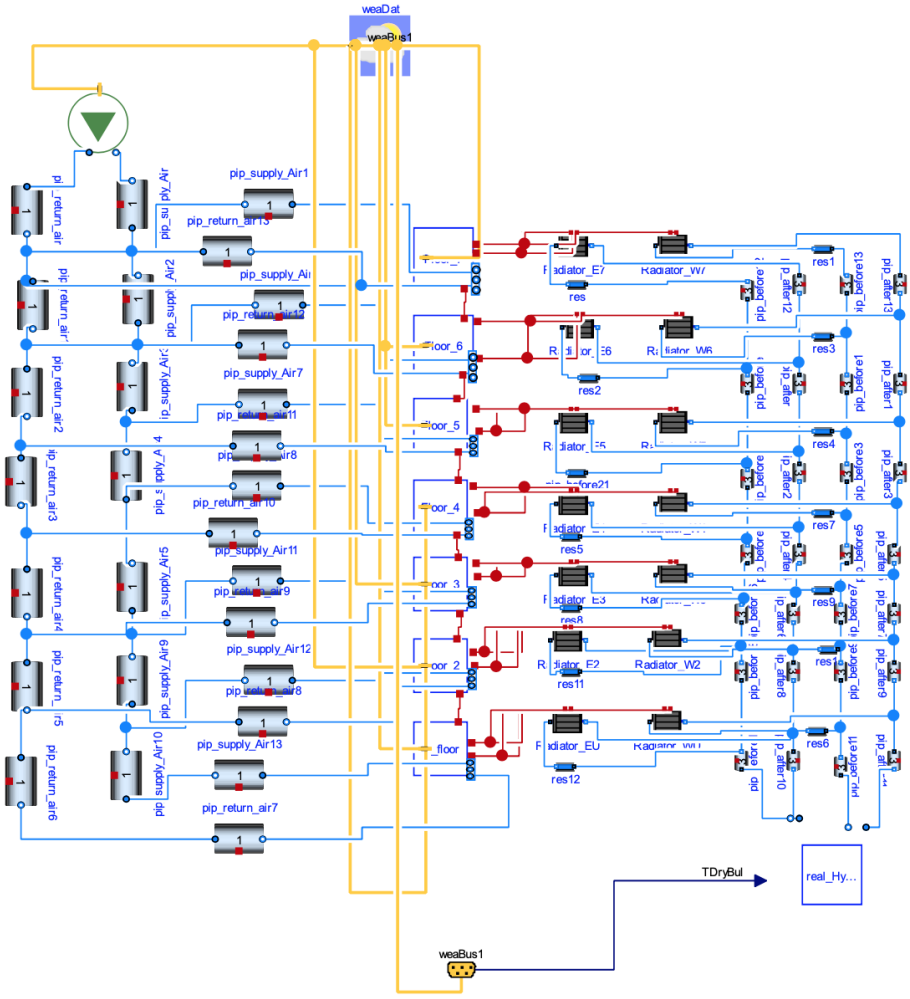

Figure 3.3: Overview of the modelled building.

Figure 3.3 illustrates the seven floors connected to the hydronic heating system which are modelled for the building. Each floor is connected to the weather data and are again connected to the floor above and below. Floor U is also connected to the ground, and 13 °C is assumed to be the outdoor temperature of the floor plate. Floor eight, not modelled, is smaller than floor seven, which results in some of the ceiling in floor seven to face the

outdoors. However, for the modelled building in Figure 3.3, it is assumed that floor eight has the same temperature as floor seven. This results in no heat flows between the two floors.

The duct and piping systems are modelled in the same manner. It is assumed that the pressure loss over each pipe is 100 Pa/m for the pipes and 1 Pa/m for the ducts. The pressure losses between the floors are assumed to be constant, therefore the diameter of the ducts and pipes change depending on how far away from the ventilation unit or hydronic heating central they are. Moreover, the pipes from the main pipe to each radiator represent the balancing valve to the radiators. It is needed to balance the pressure loss throughout the hydronic heating system. The pressure changes in the ventilation system are modelled the same way, and it is also assumed to be a 50 Pa change over the supply air terminal device. The different pressure changes and mass flows throughout the systems are presented in Tables A.3 and A.4 in Appendix A. The pipes are modelled as Mapress pipes from Geberit International Sales AG (2021).

Each floor is a separate class, and by opening one of the floors from Figure 3.3 one can observe how each floor is modelled. Figure 3.4 illustrates how the sixth floor is modelled. The sixth floor zone will be used to calibrate the internal heat gains and the nominal power for each radiator circuit. As the other floors, except the U floor, are office floors too, the internal heat gains are assumed to behave in the same manner as the calibrated sixth floor model. The nominal power for the radiators depend on the area of the floors, and will therefore be assumed to be the same power per square meter for each floor.

The connection to the weather data is seen in the component labelled ”weaBus” in Figure 3.4. From the weather data there are two components which calculates the direct or diffuse solar radiation on a tilted surface in all directions. The equivalent air temperature, as mentioned in Chapter 2.4, is also calculated in the component labelled ”eqAirTemp” in the middle part of Figure 3.4. The heat transfer between the other floors are through the red components labelled ”floor1” and ”roof1”. The connection to the hydronic heating system of the building is through the red components to the right labelled ”intGainsRad1” and ”intGainsConv1”. They represent the radiative and convective addition, respectively, to the zone from the radiators. The ventilation in Figure 3.4 is the blue component in the lower right corner. This component is connected to the ventilation as seen in Figure 3.3.

The internal gains input is the table in the lower left part of Figure 3.4, and one observes that the input is split into ”personsRad”, ”personsConv” and ”Machines” and are then added as a heat source to the zone. The internal heat gains depend on the area of each zone, which results in the U floor and second floor to have different internal heat gains than the other floors. The internal heat gains will be a part of the calibration process for the thesis in order to obtain a model in line with the real building. Lastly, the blinds are added via the gain component next to the ”roof1”-connection.

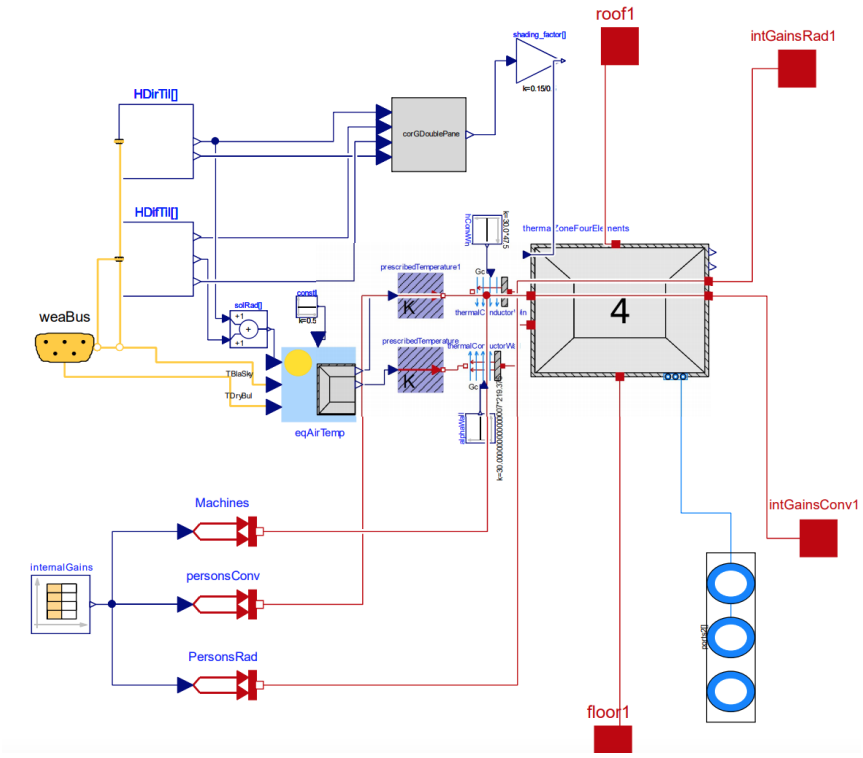

Figure 3.4: Overview of the the modelled floors.

3.4 Creating the Hydronic Heating System

The hydronic heating system supplies the U floor and the second to the seventh floor with the required heat. In the following chapter, the process of creating the hydronic heating system is presented.

3.4.1 The Connection to the District Heating Grid

The model is based on a physical building and components, where some of the nominal operating conditions are known. The outdoor design temperature in Oslo, θ_{3d}, is -19,8 °C according to SINTEF (2018). The design outdoor temperature is needed to calculate the heating demand of the building, which is needed to dimension the radiator system. The heating demand can either be found by means of manually calculating the values based on formulas from NS:3031 or data from radiator manufacturers. Moreover, the building is connected to the district heating grid in Oslo. The circulating medium in the hydronic heating system is water. The supply temperature is 80 °C at design outdoor temperature according to Fortum Oslo Varme (2018), however the building has a supply temperature of 70 °C at -15 °C outdoor temperature. The building has two water circuits for the hydronic heating system.

3.4.2 Choice of Radiators

The radiator model in Modelica is based on input data which is available from radiator producers that follow the European Norm EN 442-2 according to Lawrence Berkeley National Laboratory (2021). A conversation with Purmo, a radiator producer on the 6th of November 2020, highlighted that the properties of radiators from the 1960s are relatively similar to radiators produced in these days. Purmo therefore suggested to find the aggregated heating demand on the floor, and then divide that by the number of radiators needed on the floor and then use radiator properties from radiators produced today in the model. In Appendix A, there is an overview of the assumed number of radiators on each floor. Using this strategy and with the help of Purmo Group AS (2019), a Compact [C] radiator of the type C21 is chosen, where n = 1,2803. The specific radiator for each floor is decided by dividing the maximum power from the measurements by the number of floors, and then dividing the power on each floor by the required number of radiators per floor. By rewriting Equation 3.1 one can find the radiator constant for the system as well. K_{rad} is the radiator constant and $\Delta(T_m)$ is the arithmetic temperature difference which is explained in Equation 3.2. Lastly, n is the radiator exponent and $\dot{Q}$ is the power of each radiator.

$$\dot{Q} = K_{rad} \cdot \Delta(T_m)^n \tag{3.1}$$

The measurements and the values from the models will be compared by plotting the power of the radiators against the difference in the temperature between the radiator (T_{rad}) and the indoor air temperature, where the indoor air temperature is approximated by using the temperature of the exhaust air in the ventilation system from the measurements and the average temperature in the zones for the modelled building. This relationship is seen in Equation 3.2 and this has proven to work well with radiators. T_{supply} and T_{return} is the supply and return temperature, respectively, of the water in the radiator and T_{air} is the exhaust air in the ventilation system.

$$\Delta T_m = \frac{T_{supply} + T_{return}}{2} - T_{air} \tag{3.2}$$

3.4.3 Night Setback

The building had a night setback for the radiators during the measurement period in 2020 to avoid excessive energy use during non-occupied hours, such as during the night and weekends. When SINTEF measured the radiators they understood that the night setback of the East circuit did not operate as it should due to a malfunction in the control valve. In order to find the time for these setbacks, the supply temperature of the West radiator circuit is plotted as seen in Figure 3.5. It is decided that the time period of investigation is from 09.02.20 from 00:00 (Sunday) to 11.02.20 23:45 (Tuesday), to capture the earlier start time of the hydronic heating system at Sunday night in order to have a comfortable indoor temperature when people arrive on Monday morning.

Following the results in Figure 3.5, the night setback schedule is presented in Table 3.4. The night setback as presented in Table 3.4 is when the radiators should reduce the supply temperature by 10 °C. So when the night setback is on, the radiators will reduce the supply

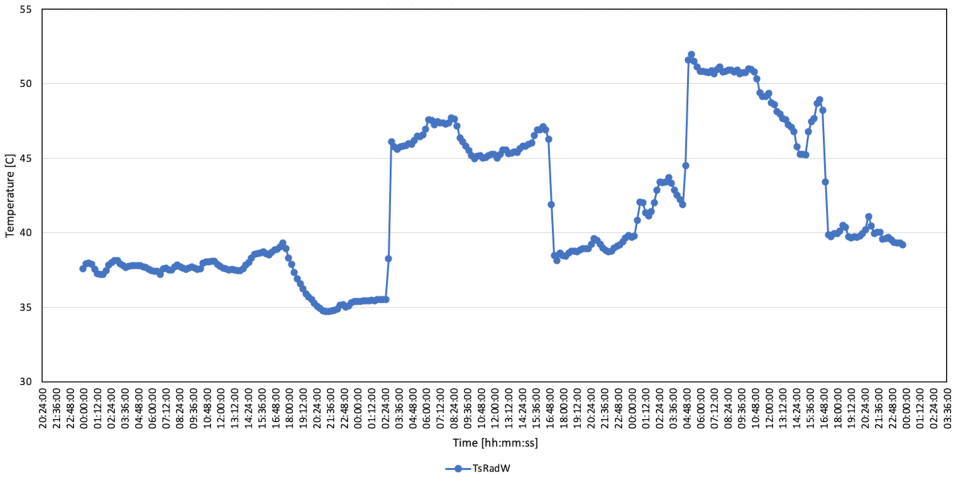

Figure 3.5: Supply temperature of the West radiator circuit.

Table 3.4: Night setback of radiators.

Day	Stop	Start
Monday	03:00	17:00
Tuesday	05:00	17:00
Wednesday	05:00	17:00
Thursday	05:00	17:00
Friday	05:00	17:00
Saturday	-	-
Sunday	-	-

temperature to the zone by 10 °C. This means that at design outdoor temperature (-20 °C), the supply temperature to the zone during night setback is 60 °C instead of 70 °C.

3.4.4 The Hydronic Heating System in Modelica

In Figure 3.6 one can observe the outline of the hydronic heating system for the zone. In Figure 3.3, the hydronic heating system is in the lower right corner. The outline of the hydronic heating systems is obtained by opening this class.

The sinks (labelled ”sin”) to the right in Figure 3.6 are a simplified method to model the function of an expansion vessel. The purpose of an expansion vessel is to allow water to flow into and out of the component in order to handle changes in the volume due to temperature and pressure changes in the system. If the sink is not present in the model, the model becomes too stiff. The heat exchanger, labelled ”hea”, in the models illustrate the connection back to the district heating network and it is needed in order to prevent that

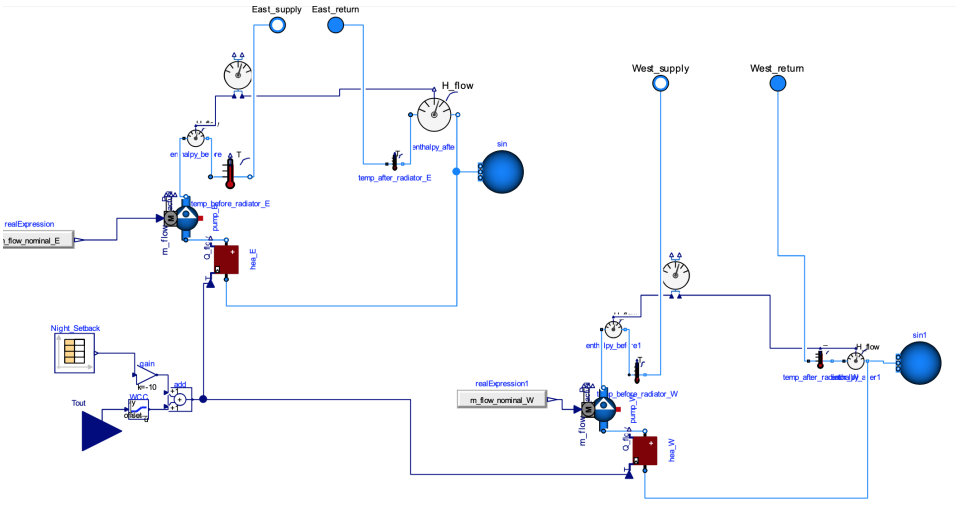

Figure 3.6: Overview of the construction of the hydronic heating system.

the radiator becomes a sink (i.e. that heat is added from the room to the radiator) during the hotter summer months, when the indoor temperature might be higher than the set-point of the radiator. The heat ports in the top part of the figure highlight how water from the hydronic heating system is distributed to the radiators in Figure 3.3.

Furthermore, the temperature sensors in the systems are needed to obtain accurate measurements in the model at that particular location to observe the temperature difference before and after the radiator. The components labelled ”enthalpy_before” and ”enthalpy_after” are connected to a component created by SINTEF Community which is called ”EnergyDiffCalc”. The ”EnergyDiffCalc” is the component just below the ports to the floors in Figure 3.6 and it is needed to calculate the power emitted by the hydronic heating system in the same manner as the power was measured in the physical building measured. The pumps in Figure 3.6 are there to move the water around in the modelled systems.

The hydronic heating system uses the outdoor temperature as an input, where the weather compensation curve is added. The weather compensation curve follows a linear relationship, meaning that at design outdoor conditions (-20°C) the water from the mass flow source will have a temperature of 70°C. The WCC is observed in the lower left corner, labelled ”WCC”. Moreover, the night setback is the schedule as mentioned in Chapter 3.4.3. The schedule contains 0’s and 1’s to illustrate whether night setback is initiated. The output of this schedule is added to the WCC, by means of the ”gain” in the model which has a value of -10.

3.5 Creating the Ventilation System

The description of the building by Walnum (2020) specifies that the Air Handling Unit (AHU) has a rotating wheel heat recovery unit and an electric reheating element. This suggests that the building has a Constant Air Volume (CAV) and temperature control of the supply temperature by means of a heating coil before the air enters the zone. The air volume is controlled by a daily schedule, as presented in Figure 3.2. The building is modelled to have a nominal air flow of 7 $m^3/(h\ m^2)$ in accordance with values from Standard Norge (2020), which is added to the Modelica model.

3.5.1 The Ventilation in Modelica

In Figure 3.7 the entire ventilation model in the Modelica model is presented.

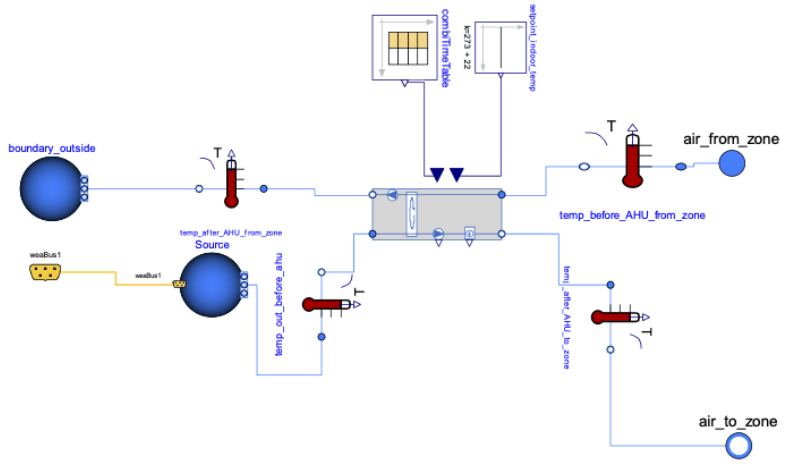

Figure 3.7: Overview of the ventilation system.

The AHU in Figure 3.7 uses the outdoor temperature as an input, the yellow component called ”weabus1”. When the outdoor air enters the AHU, it is heated by the exiting air from the zone due to the rotary heat exchanger. The table that is observed at the top in Figure 3.7 is the daily ventilation schedule in the building as seen in Figure 3.2, which is also in accordance with values from Standard Norge (2020). Moreover, to the right of the schedule is the set point for the indoor temperature, which is 22 °C during normal operation. The element called ”boundary outside” is the sink for the air exiting the building, which in reality is the outside.

The AHU in Figure 3.7 is presented further in Figure 3.8. The AHU was created by SINTEF Community.

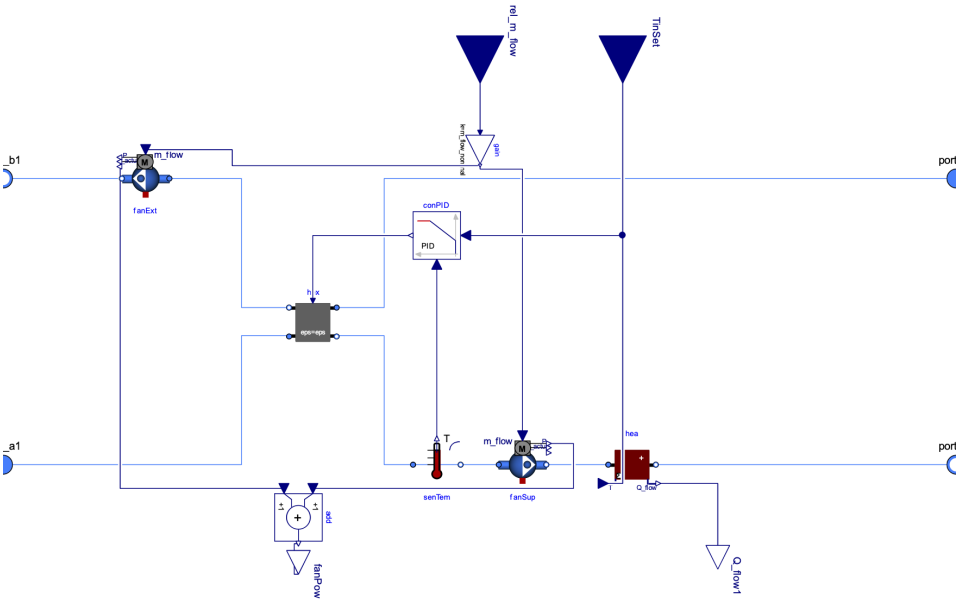

Figure 3.8: The air handling unit, created by SINTEF Community.

The rotating wheel heat recovery unit is represented by the grey heat exchanger in the middle and to the left in Figure 3.8. The daily schedule determines the relative mass flow rate through the AHU, which then represents when the rotary heat exchanger is on, and when there is only the heating coil to heat the air to the zone. The schedule is presented in Figure 3.2. The electric heating coil in the Modelica model is represented by the ”hea” component in Figure 3.8 in the right lower corner. It should also be noted that the building in Oslo has a cooling system in the AHU, however this is not modelled for the Master’s thesis.

Chapter 4

Validation and Calibration

The aim of the Master's thesis is to create an emulator of the physical building in order to test MPC algorithms on the building offline. The first step is to calibrate the model, and then apply different control strategies to the building during standard simulation conditions. The following chapter presents the validation of the meteorological data and the calibration process of the building during the measurement period.

4.1 Indices for Calibration

The American Society of Heating, Refrigerating and Air-Conditioning Engineers (2014) and U.S. Department of Energy Federal Energy Management Program (2015) highlight that there are two main statistical indices for calibration: MBE and CV(RMSE). The MBE measures how closely the values from a model corresponds to the measured data. Equation 4.1 illustrates how the MBE is calculated.

$$MBE = \frac{\sum_{period} (S - M)_{interval}}{\sum_{period} M_{interval}} \tag{4.1}$$

In Equation 4.1, M is the measured energy consumption, whereas S is the simulated energy consumption. MBE is subject to cancellation errors, and to account for such errors, the CV(RMSE) needs to be calculated too. The CV(RMSE) is the normalized spread between the sets of data. Equation 4.2 underlines how the CV(RMSE) is calculated.

$$RMSE_{period} = \sqrt{\frac{\sum(S-M)^2_{interval}}{N_{interval}}} \tag{4.2a}$$

$$A_{period} = \frac{\sum\limits_{period} M_{interval}}{N_{interval}} \tag{4.2b}$$

$$CV(RMSE_{period}) = \frac{RMSE_{period}}{A_{period}} \cdot 100 \tag{4.2c}$$

$N_{interval}$ in Equation 4.2 is the number of time intervals in the period considered. In Equations 4.1-4.2, the interval is the resolution of the measurements (one hour for the thesis) and the period is the whole time period considered (presented in Table 4.6). Table 4.1 illustrates the acceptance intervals for the statistical indices when using hourly data, according to ASHRAE.

Table 4.1: Acceptable values for statistical indices using hourly data

MBE	$\pm$ 10 %
CV(RMSE)	$\pm$ 30 %

For each model presented in Chapter 4.7, the MBE and CV(RMSE) are calculated to ensure that the models are calibrated.

4.2 Measurements

SINTEF measured the values of the building in Børrestuveien from the 27th of December 2019 until 15th of April 2020. However, from the 27th of December until the 6th of January the supply temperature of the radiator in the East radiator circuit ranged from 2180 to 3276 °C which is far beyond correct temperature. Moreover, the measurements of the different temperatures in the various rooms in the building only started on the 7th of February. Therefore, it is decided to only investigate the data after 7th of February until the end of the measurement period, which is the 15th of April 2020.

During the time period of measurements, SINTEF decided to perform an experiment during the Easter holiday. A Pseudo-Random Binary Signal (PRBS) experiment was set up to obtain information about the building's response in order to create a model of the building. Table 4.2 highlights the experiment set up.

The last two points in Table 4.2 are needed to ensure that the radiators are really off during periods when they should be off according to the PRBS. The experiment period is from the 6th of April 2020 to the 15th of April 2020.

Table 4.2: PRBS experiment set up.

Ventilation schedule	67% load 24/7
Ventilation set point	20 °C
WCC radiator	70 °C
Night setback radiator	20 °C

4.3 Meteorological Data

The specialization project highlighted the need for customized weather data for the model in order to calibrate the modelled building, meaning the weather data of the particular time period of measurements. It is insufficient for the model to have standard weather file for Oslo as it is not comparable to the measured weather. The ”typical weather” file contains weather data from various years, and the ”typical weather” file as a whole should represent a normal year in Oslo. However, the measurements from the physical building are from the time period from 07.02.20 to 15.04.20. Therefore a weather file from the same year needs to be considered in order to simulate the building in the same conditions as the actual building experienced.

4.3.1 Measurements at Blindern

Data from the meteorological station at Blindern made available by Norsk Klimaservicesenter (2021) will form the foundation to create the weather file for the calibration process for the modelled building in Modelica. A Python script developed by SINTEF will determine the solar components for the weather file. The script calculates the DHI and DNI components, as well as the dew point temperature and creates a spreadsheet with the new values. Table 4.3 illustrates the required input parameters from the weather station at Blindern to the script developed by SINTEF.

Table 4.3: Input parameters from Blindern weather station.

Input	Unit
Relative humidity	-
GHI	W/m^2
Air temperature	°C
Pressure	hPa
Wind direction	°
Wind speed	m/s

4.3.2 Solar irradiation

The station has information about the global solar irradiation, but Modelica requires two components for its model: the direct normal irradiance and the diffuse horizontal radiance. As presented in section 2.6, the measurements of the global horizontal irradiation are used to calculate the direct normal and the diffuse horizontal components. The power from the sun that reaches the surface of the earth is 1000 W/m^2 on a clear summer day according to Hofstad (2020). Rossing et al. (2020) claim that 800 W/m^2 is the typical power on the surface of the earth in Norway on a summer day. In Figure 4.1 the GHI at the weather station at Blindern is observed.

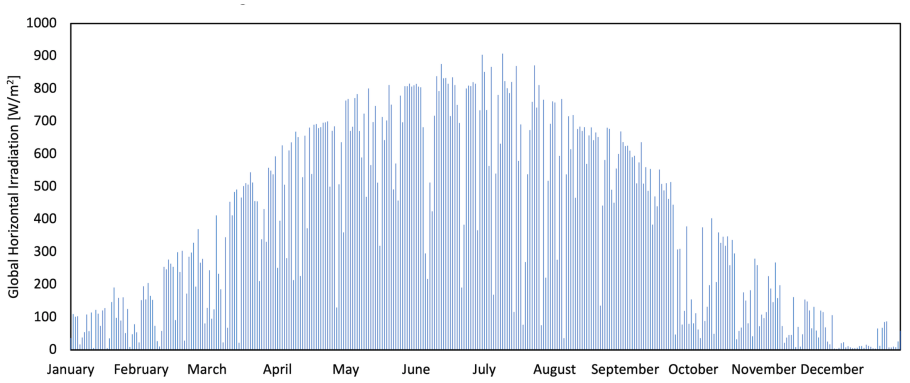

Figure 4.1: Measurements of the global horizontal irradiation at Blindern in 2020.

The measured GHI presented in Figure 4.1 is in line with values presented in the literature, and is always less than 1000 W/m^2 and some days above 800 W/m^2 during the summertime.

4.4 Creating the Weather File

The weather file is created by following a recipe from SINTEF which utilizes a Python script provided by SINTEF. Next, the results from the script are added to an existing weather file in a spreadsheet and finally a *.epw*-file is created. The *.epw*-file is the Energyplus weather file format. The *.epw*-file is converted to a *.mos*-file. This format for the weather file is required when inserting the weather file in Modelica. The following section will describe the methodology of creating the weather file in more detail.

4.4.1 PVLib

The PVLib library is created by Holmgren et al. (2018) to simulate the performance of photovoltaic systems. SINTEF created a script based on the PVLib library, in order to obtain the DHI and DNI values from the GHI values as well as to calculate the dew point temperature. An overview of the functions from the PVLib libary utilized for the script is observed in Table 4.4.

Table 4.4: Classes and functions from PVLib

location.Location(latitude, longitude[, tz, ...])
solarposition.spa_python(time, latitude, ...)
location.Location.get_clearsky(times[,...])
irradiance.dirindex(ghi, ghi_clearsky,...)
irradiance.erbs(ghi, zenith, datetime_or_doy)

The script requires the location parameters in Table 4.5 to create a location object (Oslo) as well as the input parameters presented in Table 4.3 to calculate the input to the weather file. The pressure presented in 4.5 is the average air pressure at Blindern in 2020.

Table 4.5: Location parameters Blindern

Altitude	94 m
Longitude	10.7200°
Latitude	59.9423°
Pressure	99811 Pa
Timezone	Europe/Oslo

Solar Position Algorithm

The values from Table 4.5 are required by the NREL Solar Position Algorithm (SPA) created by Reda and Andreas (2004) to calculate the solar zenith angle. The algorithm created by the authors should produce the solar zenith and azimuth angles with uncertainties around $\pm$0,0003°. The solar zenith angle is presented in Section 2.6, and as observed from Table 4.4 it is required in the calculation of irradiance.

Clear Sky Estimates

The clear sky function is a method to calculate the GHI, and DHI at the particular location utilizing SPA in the PVLib library by Holmgren et al. (2018) and Holmgren et al. (2021). The clear sky function accepts either ineichen, haurwitz or simplified_soils as a clear sky model input. Reno et al. (2012) concluded that the ease of application and the good performance of the ineichen model makes it the recommended solution for most locations. The ineichen clear sky model is included in the clear sky function in the script in the Master's thesis.

Solar Irradiance Calculations

In the PVLib library, there are two models to calculate the DNI: the erbs model and the dirindex model. Following the results from said models, the DHI can be estimated. The

dirindex model is developed by Perez et al. (2002) to calculate the clear sky global and direct irradiance, find the cloud-index-to-irradiance index and convert global to direct irradiance. The authors validated the model against various locations and concluded that the dirindex model was an improvement to existing models at the time at all locations tested in the report. To ensure validation of the dirindex model, the DNI and DHI for Fornebu and Blindern are calculated and presented in Figure 4.2.

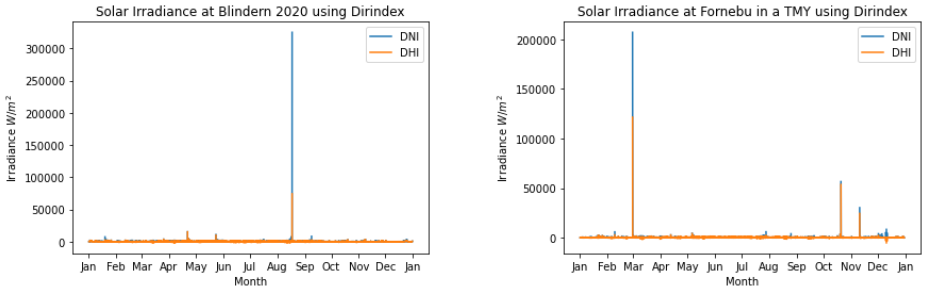

(a) DNI and DHI at Blindern in 2020.

(b) DNI and DHI at Fornebu in a TMY.

Figure 4.2: Results using the Dirindex model.

It is evident from both Figure 4.2a and 4.2b that the dirindex model obtains extreme values at certain dates. According to Hofstad (2020), the maximum irradiance at the earth's atmosphere is around 1370 W/m^2. The model has values above this value 197 times for the Blindern weather and 159 times for the Fornebu data. The Dirindex results also respectively give 123 and 127 infinity values for the Fornebu and Blindern data.

The Erbs model estimates the DHI using Equation 2.6 and was established by Erbs et al. (1982). Following the results from Equation 2.6, the DNI is obtained from Equation 2.5. The results from the Erbs model at Blindern and Fornebu are presented in Figure 4.3 for comparison.

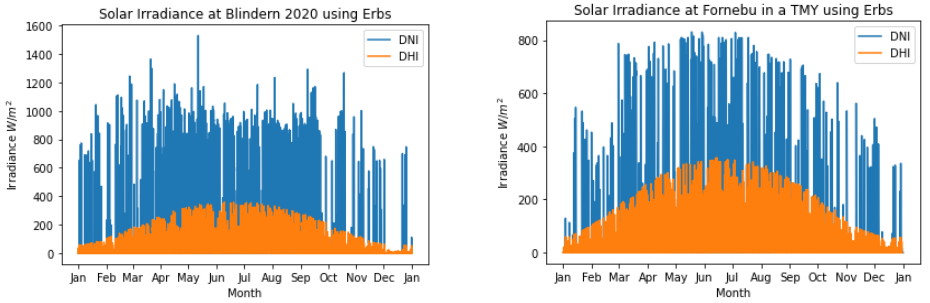

(a) DNI and DHI at Blindern in 2020.

(b) DNI and DHI at Fornebu in a TMY.

Figure 4.3: Results using the Erbs model.

The results at the two location with the Erbs model depict that the data from Fornebu have no values above the possible irradiance level and and no infinity value. The weather data from Blindern have 1 value above 1370 W/m^2 and no infinity values. For the Master's thesis, it is therefore concluded to that the Erbs model will be the designated solar irradiance calculation model.

4.4.2 Energyplus Weather File

The Python script creates a *.txt*-file containing the time, outdoor temperature, wind speed, wind direction, relative humidity, pressure, GHI, DNI, DHI and the dew point temperature at Blindern in 2020. Additionally, the original *.epw*-file of the TMY at Fornebu is converted to a *.csv*-file. The content of the *.txt*-file from Python is then added to *.csv*-file of the TMY in Fornebu to ensure compatibility with the required format for the conversion to a *.epw*-file. The EnergyPlus WeatherConverter converts the *.csv*-file of Blindern in 2020 to the required *.epw* format. The new *.epw*-file is then converted to a *.mos*-file to be added to Dymola.

The weather data from Blindern is from 2020. 2020 was a leap year, and the TMY data do not account for the additional day. To create values for the cells where there are no measurement data, the average of the values in the TMY file on the 28.02 and the 01.03 at the same hour is used. However, when converting the *.epw*-file to *.mos*-file and simulating the model, it is clear that the additional day due to a leap year causes the simulation to terminate unsuccessfully. Therefore, it is decided to omit the measurement data for the weather from 29.02.

4.5 Modifications due to Removal of the data from 29th of February 2020

The conversion in from *.epw*-file to *.mos*-file when including 29.02 was unsuccessful, and to avoid this problem, the weather data from that date are neglected. This creates a need for more modifications in the model, since many of the variables are influenced by the day of the week. Thus, the internal heat gain schedule and the ventilation schedule are updated to ensure that the schedules correspond to the applicable day of the week, after the removal of the 29th of February.

The data collected from the building that is viable for comparison is from 07.02.20 to 15.04.20. In order to encompass as many dates as possible for investigation, the two periods before and after the 29th of February are divided as presented in Table 4.6.

Period 2, as presented in Table 4.6, starts at the second of March, to allow the building to reach an equilibrium. This is needed as the removal of the 29th of February causes abrupt changes to the data from the weather file, as well as the tables containing measurements from the physical building.

Table 4.6: Comparison periods

	Start	Stop
Period 1	07.02.20	28.02.20
Period 2	02.03.20	12.03.20
Period 3	13.03.20	06.04.20
Period 4	06.04.20	15.04.20

4.6 Validation of Meteorological data

Validation of the meteorological data is important in order to ensure that the model experiences the same outdoor conditions as the building. In this chapter, the comparison of the outdoor temperature and the global solar radiation are presented. The comparison of the remaining parameters between the model and the measurements are presented in Appendix B. In Figure 4.4 one observes how the temperature in the weather file and the measured temperature vary.

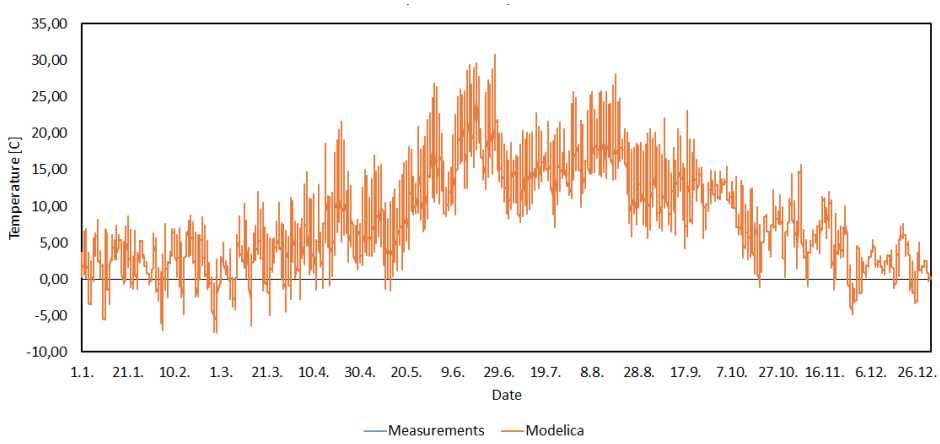

Figure 4.4: Comparison of the outdoor temperatures.

It is evident that the implementation of the measured outdoor temperature to the weather file was successful based on the results in Figure 4.4. There are no deviations between the temperature experienced by the model and the measurement data.

Figure 4.5 highlights the differences between the measured global solar radiation at Blindern to the values created SINTEF's Python script.

From Figure 4.5 it is clear that there are some variations between the global radiation of the measurements and the simulated values. The reason is discovered in the documentation of the TMY3 reader by OpenModelica (2021). Global radiation measurements used to

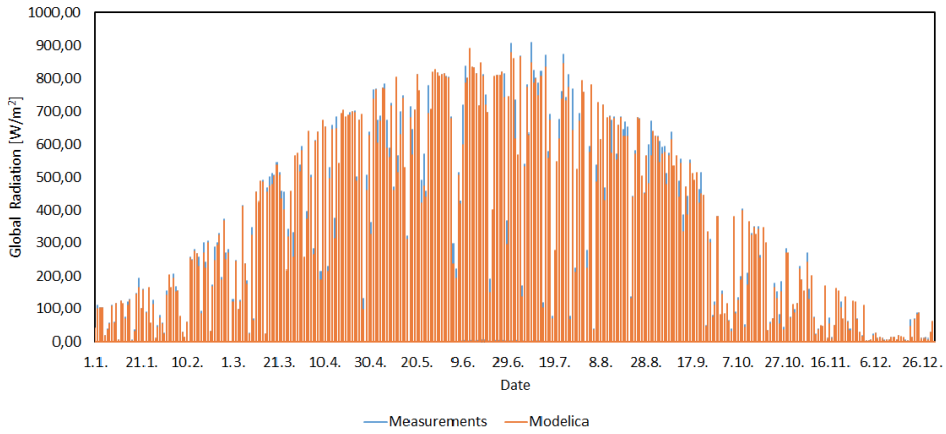

Figure 4.5: Comparison of the global radiation.

create TMY3 files are measured as the sum of the solar radiation on a surface aggregated over one hour and added to the following hour. Thus, the TMY3 reader will shift the solar radiation 30 minutes prior to the time stamp of the measurement, to obtain a more accurate interpolation. The measurements of solar radiation from Blindern are also measured in the same manner as one does for the TMY3 file. Therefore it is assumed that the resulting global radiation from the Modelica model will be more in line with how the actual solar radiation is perceived by the building.

4.7 Models for the Calibration Process

The calibration process is first performed on one floor of the building, the sixth floor, to reduce simulation time and obtain a clearer image of the sources of errors as there are fewer variables and parameters in one floor. Following the calibration of the floor, the same parameters will be extended to the entire building. The goal is that the parameters resulting in a calibrated sixth floor will ensure that the entire building is calibrated.

4.7.1 Model 1 - The Sixth Floor

Model 1 is the sixth floor of the building, which is the same floor that was modelled for the specialization project. The modelled zone is presented in Figure 4.6.

The green triangle in the lower left corner of Figure 4.6 represents the ventilation system. Instead of a fixed set point temperature in the ventilation system, as seen in Figure 3.7, the set point temperature is now in a table in order to ensure that the set point temperature will be 20 °C during the experiment period. The hydronic heating system is presented in the upper right corner, with one class for each of the two circuits. The weather data is added to the component in the upper left corner labelled ”weaDat”. The area of the interior walls are estimated to be 926,1 m^2, based on measurements of the sixth floor drawing in

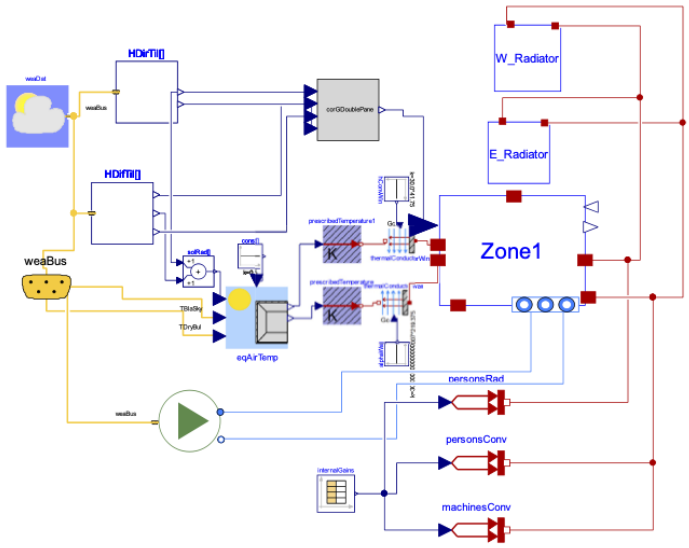

Figure 4.6: Model 1 - the sixth floor of the case building.

Appendix A. It is assumed that there is one radiator in each of the cell offices meaning that there are 20 radiators on the floor. The average power emitted in each room is 402 W, therefore a Purmo C21 with a length of 600 mm is chosen. Each C21 radiator has a nominal power of 427 W and n = 1,2803.

The assumption is that the sixth floor model is representative for the other floors too. The floor and ceiling are assumed to be adiabatic, as seen in Figure 4.6, where the nodes representing the floor and the ceiling are not connected to anything. This is a simplification to the real building, but as the temperatures in floor five and seven are approximately the same as the temperature on the sixth floor it is an appropriate simplification for the calibration process.

4.7.2 Model 2 - The Building

Model 2 is the entire building. It has only one consumer substation connected to the district heating grid, and the ventilation system is scaled up. The outline of the model is identical to the model in Figure 3.3. The difference between the model in Figure 3.3 and Model 2 is the weather data used in the model and the tables added to the model. Model 2 uses the internal heat gain tables obtained from calibrating Model 1, schedule for ventilation and input data for the mass flow rate and supply temperature from the measured data of the physical building. The weather data in Model 2 is the weather at the Blindern measuring station in 2020, as explained in more detail in Chapter 4.3.

4.8 Methodology of the Calibration Process

There are two parameters to be calibrated in the modelled building - the nominal power per radiator circuit and the internal heat gains. Table 4.7 illustrates the intervals considered for the calibration process.

Table 4.7: Intervals considered for calibration.

Interval name	Start date	Start time	Stop date	Stop time
Period 1	07.02	00.00	28.02	23.00
Period 2	02.03	00.00	12.03	23.00
Weekend 1.1	13.03	19.00	14.03	05.00
Weekend 1.2	14.03	19.00	15.03	05.00
Weekend 1.3	15.03	19.00	15.03	05.00
Weekend 2.1	20.03	19.00	21.03	05.00
Weekend 2.2	21.03	19.00	22.03	05.00
Weekend 2.3	22.03	19.00	23.03	05.00
Weekend 3.1	27.03	19.00	28.03	05.00
Weekend 3.2	28.03	19.00	29.03	05.00
Weekend 3.3	29.03	19.00	30.03	05.00
Weekend 4.1	03.04	19.00	04.04	05.00
Weekend 4.2	04.04	19.00	05.04	05.00
Weekend 4.3	05.04	19.00	06.04	05.00
Full weekend 1	13.03	19.00	16.03	05.00
Full weekend 2	20.03	19.00	23.03	05.00
Full weekend 3	27.03	19.00	30.03	05.00
Full weekend 4	03.04	19.00	06.04	05.00
Experiment	06.04	00.00	15.04	08.00
Measurement	07.02	00.00	15.04	08.00

It is evident from Table 4.7 that most of the intervals are after 12.03. This is because at this time one can assume that there are no people present in the building, thus removing one parameter to tune for the calibration process. The goal of the calibration process is to obtain values for the internal heat gains and the radiators' nominal power so that the model and the physical building behave in the same manner.

4.8.1 The Radiators

The main goals of the model in Modelica are to obtain an indoor temperature within acceptable levels from the measurements and to ensure that the model's behaviour resembles that of the physical building. To obtain such a model, some results from the measurements will be used in the model to reduce the number of variables to be calibrated. Therefore, the measured mass flow rate and supply temperature to each radiator are added as tables to the

hydronic heating systems for the measurement period. Before and after the measurement period, the average value of each data series is added.

Moreover, during the experiment, the radiators are shut off at different intervals. The radiators in the building were controlled by a set point temperature during the experiment, and to ensure that the modelled radiators operated in the same manner the supply temperature of the radiators are set to 10°C when the power from the measurements are below 0 W.

The model and the building contain an East and a West radiator circuit. In the model, these are both added and it is assumed that they supply half of the modelled zone each with the required power. By tuning the nominal power (W/m^2) added by each radiator, the model is calibrated by following the indices presented in Chapter 4.1. The calibration process follows the flow as presented in Figure 4.7.

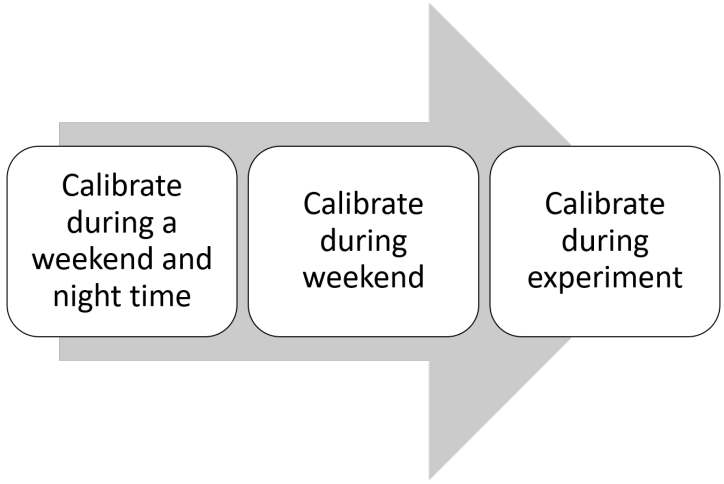

Figure 4.7: Flow chart for the calibration process.

The purpose of the flow chart presented in Figure 4.7 is to ensure that all of the intervals are calibrated and to increase the complexity at each step. The first step is to calibrate the model during the night time and during the weekend, when it can be assumed that there are no people present and no influence from the sun. At this time, there will only be heat transfer between the building and the outdoor due to the difference in between the indoor and the outdoor temperature. The next step is to calibrate during the weekend, when it is assumed that there are no people present but solar gains are considered during the daytime. The final step is to calibrate during the experiment period that took place from 06.04 to 15.04. A detailed overview of the intervals considered for the calibration process is presented in Table 4.7.

The calibration process for the sixth floor is explained in the Chapter 4.9. The same procedure is applied to the entire building, although the calibration process for the building will not be explained in such extensive detail.

4.9 Calibration of One Floor

The designated floor for the calibration process is the sixth floor of the building, and it is used for the calibration process to obtain information about the assumed internal heat gains schedule and the nominal power for each radiator circuit. The first step is to calibrate the building in terms of power consumption. From the specialization project, it was known that the nominal power of the hydronic heating system is around 29 W/m^2. Therefore, by means of trial and error around this value, the West circuit has a nominal power of 35 W/m^2 and the East circuit has 25 W/m^2.

The first step of the calibration process tested if it could be assumed that the modelled building and the physical building had internal heat gain values as presented in Standard Norge (2020). The initial tests proved that the model was yet to be calibrated, according to the tolerances presented in Table 4.1. An assumption from the first simulation is that there is no loss in the system between the location where the measurements took place, and the radiators. The measurement of the power in the physical building is in the heat central, where the district heating network meets the building. A conservative assumption is a 10% loss in the system. This assumption is used for the next simulations.

Moreover, a more accurate representation of the internal heat gains for this model is to remove the heat added by people from the 12th of March 2020 and reduce the heat by equipment and lights to the minimum load as seen in Figure 3.2. It can be assumed that there are no people in the building and the machines and lights will therefore not increase nor have the same variation as seen in Figure 3.2. The load profile for people will therefore be 0 and equipment and lights will be 0,09 from the 12th of March until the end of the year. 0,09 is the minimum load from Figure 3.2 for lights and equipment. These assumptions are deemed appropriate as the COVID-19 pandemic hit and Norway close down on the 12th of March 2020. The model greatly improves, as the heat gains due to people and equipment are reduced when the week starts which illuminate that the internal gains during the weekend are acceptable. Figures 4.8 and 4.9 highlight the final simulation results.

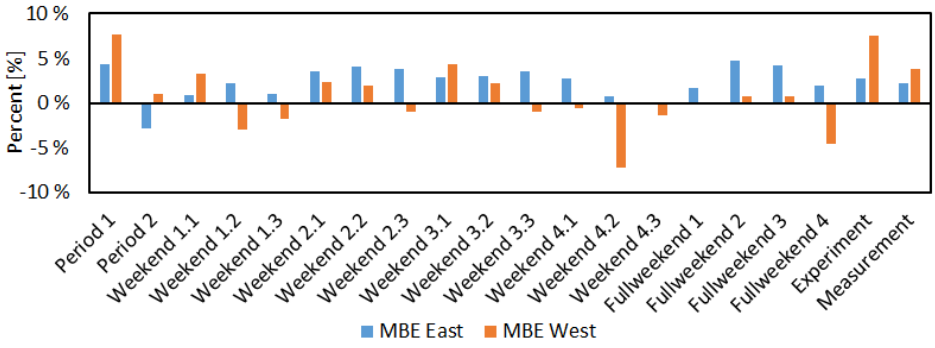

Figure 4.8: MBE of the power consumption for the sixth floor.

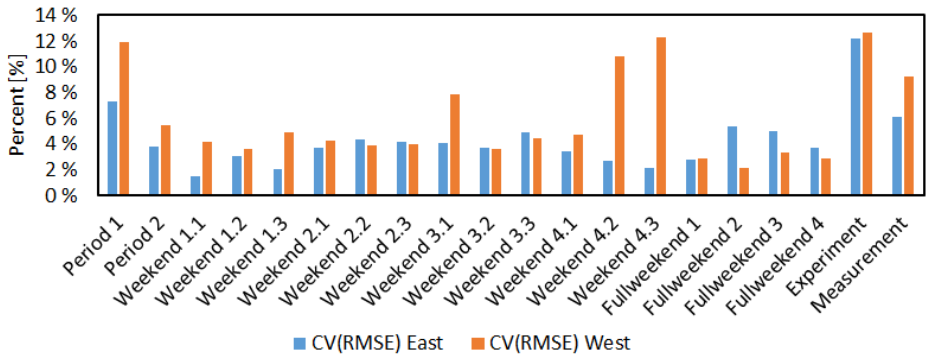

Figure 4.9: CV(RMSE) of the power consumption for the sixth floor.

In Figures 4.8 and 4.9 it is evident that the model is within the tolerance levels presented in Table 4.1. The model is therefore calibrated with respect to power consumption.

4.9.1 Results during the PRBS Experiment in the Sixth Floor

The next step is to ensure that the indoor temperature in the modelled building is within acceptable levels from the measured indoor temperature. The focus is to ensure that the model responds to changes in the radiator power in the same manner as the physical building does. Furthermore, the ventilation system was running at all times during the experiment period. This ensures that one avoids that the model assumes a constant temperature which occur when the ventilation system is not running. Therefore, it is decided to investigate the experiment period when considering if the indoor temperature is acceptable. Figure 4.10 highlights the temperatures during the experiment period from 06.04.20 to 15.04.20. The temperature measurements from the sixth floor are averaged as the weighted average of the measured temperatures to the number of rooms where one can assume the same temperature.

A general observation from Figure 4.10 is that the internal gains from Standard Norge (2020) are too high at the start of the experiment as seen from the data line labelled ”IG100”. ”6_avg” is the average temperature from the measurements of the building. The other two data series, ”IG100_noppl” and ”IG90”, are 100% of the values in Standard Norge (2020) and 90% respectively. The scenarios also assume that the heat emitted to the zone by the machines are reduced and that no people are present in the building after the 12th of March. The difference between no reduction in the internal gains (”IG100_noppl”) and 10% reduction in the internal gains (IG90) does not influence the indoor air temperature during the experiment to a great extent. It is evident from Figure 4.10 that the temperatures do not perfectly overlap, however the main goal is to have the same response in the model as the physical building has.

It can also be seen from Figure 4.10 that the start temperature in the experiment interval

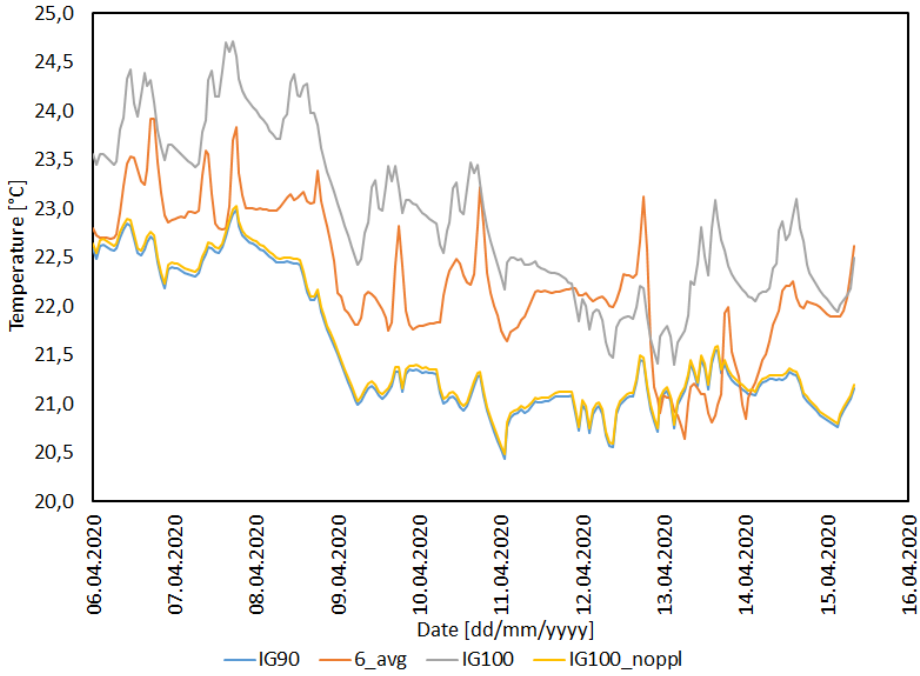

Figure 4.10: Indoor air temperature during experiment for the different scenarios in the calibration process. ”6_avg” is the average temperature from the measurements of the building. ”IG100_noppl” and ”IG90” are 100% of the values in Standard Norge (2020) and 90% respectively, with no people and minimum heat added by equipment and light. ”IG100” is the values from Standard Norge (2020).

of the ”IG100_noppl” data are more similar to the average temperature (”6_avg”) than the other data series. This indicates that the model is calibrated during the night and weekend, as the heat added to the modelled zone and the building are of the same magnitude which results in a similar indoor air temperature.

In Figure 4.10 one observes how the temperatures vary in the zone at different times. However, one needs to consider the factors influencing the indoor air temperature. Figure 4.11 presents the main result parameters from floor six during the PRBS experiment.

In Figure 4.11a at 09.04 the indoor air temperature in the zone falls sharply. Figure 4.11c explains this decrease, as the radiators are turned off at this time. As mentioned in Chapter 4.8.1, the temperature supplied to the system whenever the radiators are off during the PRBS experiment is set to 10 °C to ensure that the radiators are off. This results in spikes in the power used by the radiators at various intervals in Figure 4.11c, as extra power is needed to heat the water circulating in the system.

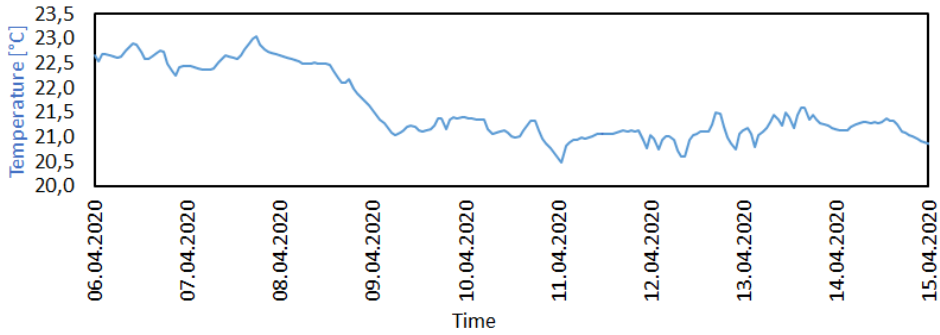

(a) Temperature on the modelled sixth floor over the PRBS experiment.

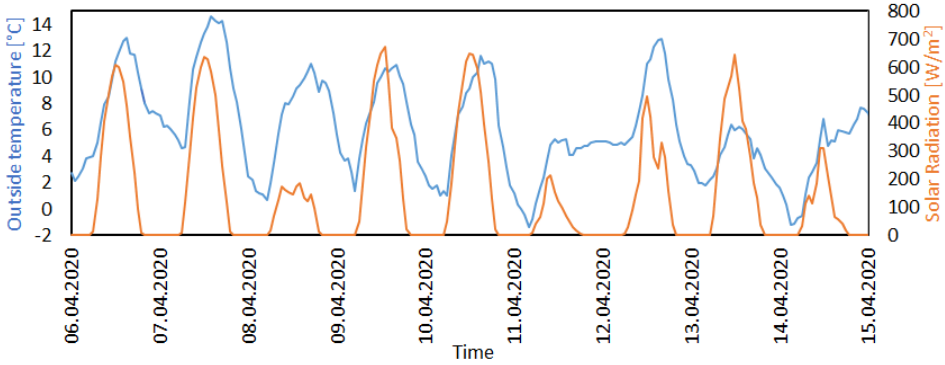

(b) Weather parameters.

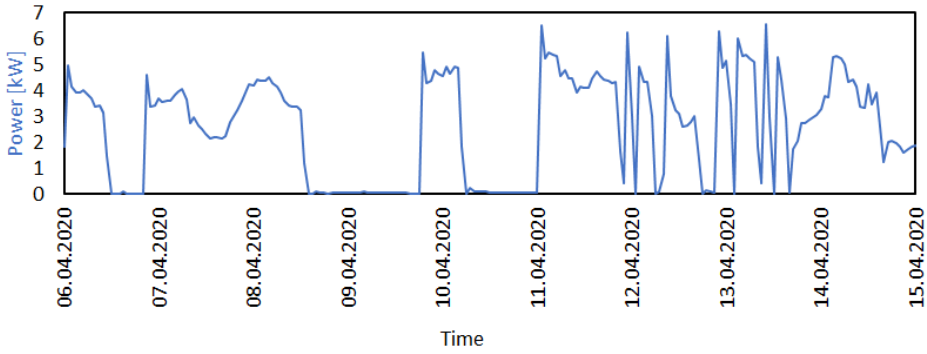

(c) Power consumption.

Figure 4.11: Results during the PRBS experiment for the modelled sixth floor.

4.10 Calibration of the Building

Following the calibration of the sixth floor, the calibration process is continued to the entire building. The aggregated power by the East and West circuits are presented. The aggregated power of all the floors measured in each of the circuits in the heating central is considered for the calibration process. The results of the calibration process, with the same inputs as were added to the model of the sixth floor, are presented in Figures 4.12 and 4.13.

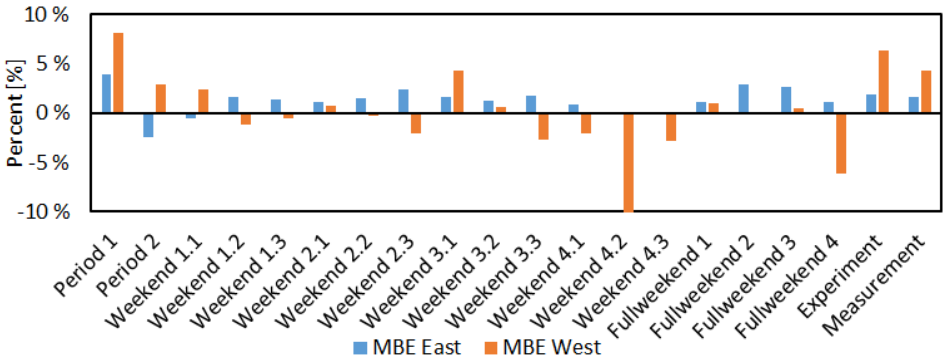

Figure 4.12: MBE of the power consumption for the whole building.

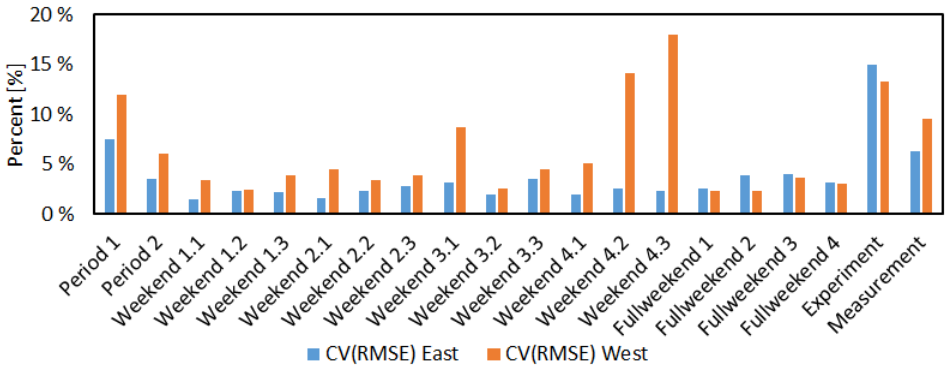

Figure 4.13: CV(RMSE) of the power consumption for the whole building.

It is evident from Figures 4.12 and 4.13 that all of the intervals are calibrated according to the MBE and CV(RMSE) tolerance intervals in Table 4.1. Moreover, the indoor air temperature of the various zones in the building should be investigated to ensure that the indoor climate is acceptable.

4.10.1 Indoor Air Temperature

The indoor air temperature of all the zones are compared to the extract temperature called ”SU-7A” from the measurements by SINTEF Community. ”SU-7A” is the extract temperature in the AHU on the roof in the measured building and includes the floors from U to seven. There is some uncertainty as to whether this temperature includes the extract air from the first floor too. However, a fair assumption is that the indoor air temperature in the first floor is not too different from the temperatures in the U floor or the second floor thus not impacting the extract air temperature to a great extent. Figure 4.14 presents the results from the simulation and measurements during the experiment period.

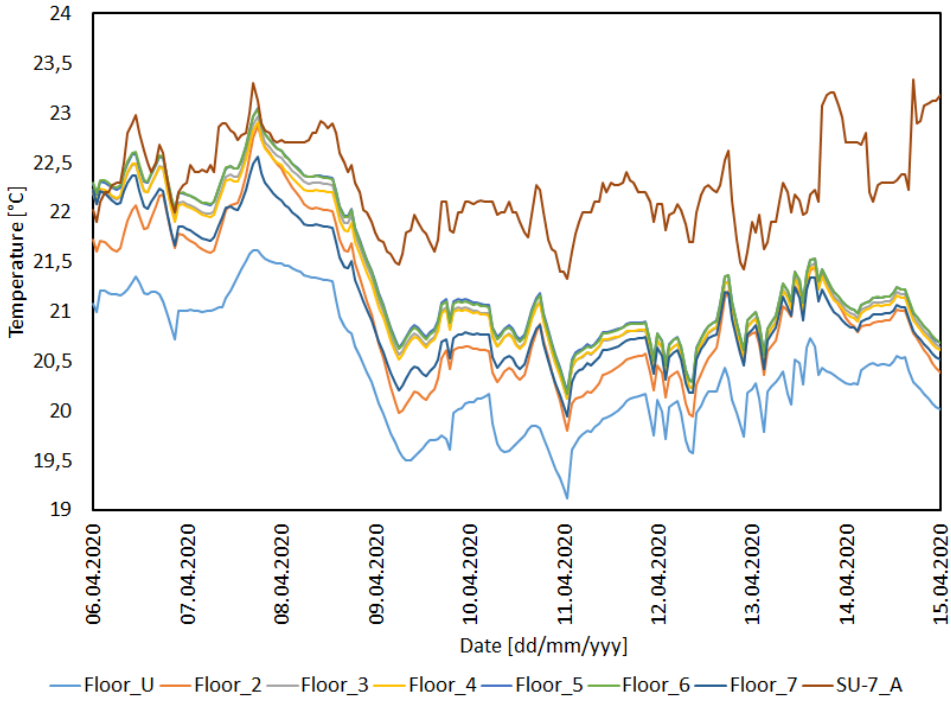

Figure 4.14: Comparison of simulated and measured air temperature in the extract duct of the building.

The comparison of zone air temperatures for the modelled and the physical building in Figure 4.14 coincide with the results from the sixth floor presented in Figure 4.10. It is evident in Figure 4.14 that ”Floor_U” is connected to the ground and has lower internal heat gains than the other floors due to its lower temperature. The lower zone air temperature in ”Floor_U” results in a lower air temperature in ”Floor_2” as these two are connected in Figure 3.3.

4.10.2 Radiator Power of the Calibrated Building

The measured parameters from the building are compared to the calibrated model of the entire building to investigate how they differ. Both the measurement data and the calibrated model use weather data from 2020, and the calibrated model use direct inputs from the building. The relationship between the radiator power and the temperature difference between the radiator and the ventilation extract is presented in Figure 4.15.

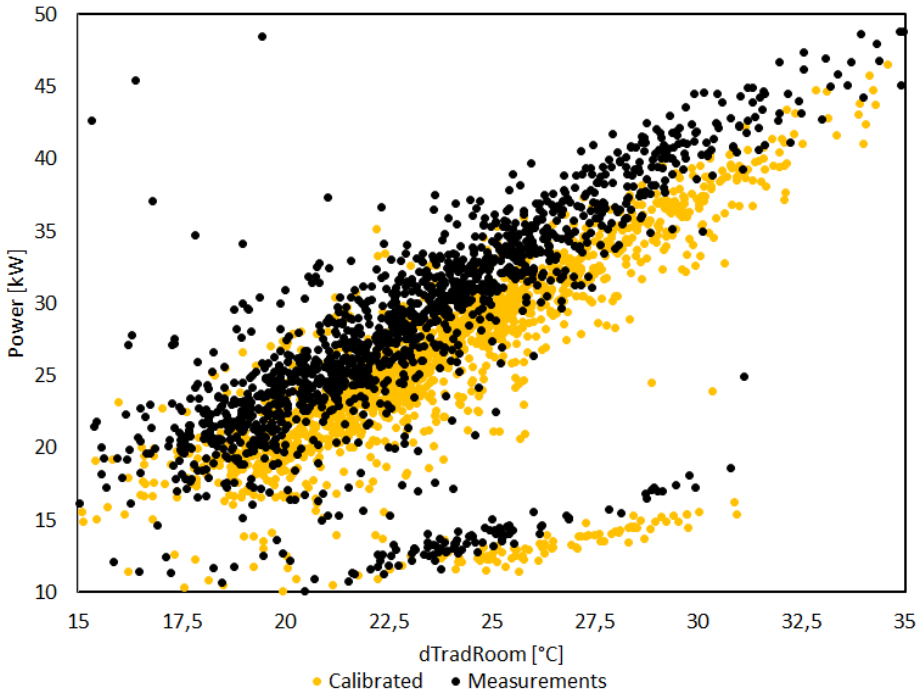

Figure 4.15: Comparison of the difference between the radiator power and the difference between the radiator and indoor temperature between the calibrated model and the measured building.

The calibrated model has generally a lower power use for the same temperature differences between the radiator and extract air temperature than the measured building has in Figure 4.15. The temperature difference considered for Figure 4.15 is found by subtracting the exhaust air temperature in the air handling unit from the weighted average of the radiator temperature where the weights are proportional to the East and West circuits' emitted power.

4.11 Analysis and Discussion of the Calibration Process

The calibration for the thesis was performed by altering the internal gains and changing the nominal power of the radiators. There can be model error in the when comparing the measured data to the simulated data, as described by Royapoor and Roskilly (2015), relating to the simplifications during the modelling process.

4.11.1 Blinds

The blinds in the model are based on a photograph of the actual building in May 2020. The building is located in Oslo and during the COVID-19 pandemic a work from home policy was enforced. It is predicted that no people were present in the building from the 12th of March until the end of the measurement period, and also when the photograph was taken in May. The implication of this assumption is that the position of the blinds in the photograph are identical to the position people left the blinds in when they left the office on the 12th of March. This assumption is extended further and applied to the model during the whole year. A sensitivity analysis is performed for the modelled building during a year of normal operation in Chapter 5.4 to investigate the effects of the assumed level of blinds.

4.11.2 Radiator Power

The results presented in Chapter 4.10.2 highlight differences between the calibrated model and the measurements in terms of radiator power. It is clear that the emitted power by the radiators in the physical building is higher than the calibrated model at the same temperature differences. An explanation of this can be that it is assumed that the air in the modelled building is perfectly mixed in the zone, whereas the physical building can have local hot and cold spots.

4.11.3 Separation of Measurement Period

During the development of the weather file, it became evident that it was difficult for the Modelica model to account for a leap year. The solution was to separate the measurement period into a period before the 29th of February and one after. For all the tables created for the model, as presented in Figures 3.4, 3.7 and 3.6, the 29th of February was simply removed. The process of removing a date creates a discontinuity in the input data for the model, which creates a need to allow the model 24 hours to absorb the aforementioned discontinuity. Figure 4.16 highlights the impact on the weather data input to the model.

Time zero in Figure 4.16 is 28.02.20 at 00:00, and it is clear in the graph that from hour 23 to 24 there is an abrupt change in the temperature. This is where the data for the 29th of February is removed. Following the sudden adjustment in the outdoor temperature from 23 to 24 on the 28th of February, the calibration process is not considering the first day after this change. The building time constant for heavy buildings range from 50-200 hours. However, since the modelled building was not completely charged or discharged following this change and the air changes per hour (ACH) in a building before 1985 is six

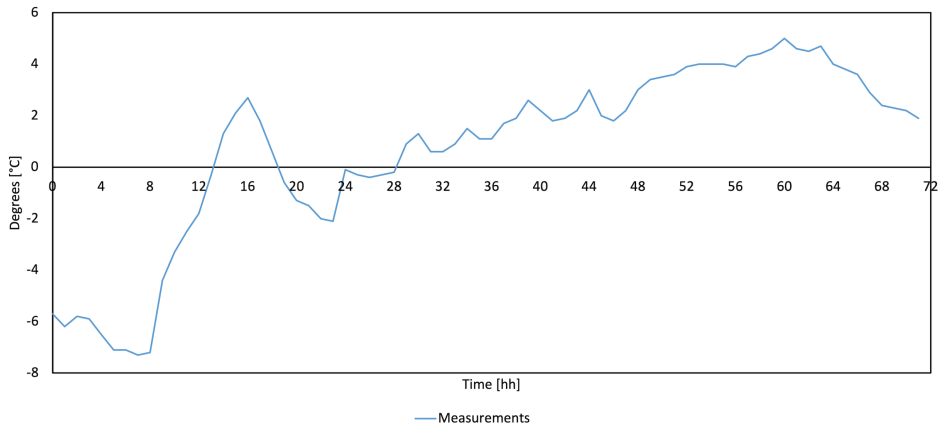

Figure 4.16: Overview of the discontinuity in the weather data between 28.02.20 and 01.03.20.

ACH according to Standard Norge (2020), it is considered sufficient to give the building 24 hours to adjust to the sudden change in the outdoor temperature.

4.11.4 Internal Heat Gains

The specialization project revealed the need for updated internal gains for the modelled building. Royapoor and Roskilly (2015) state that the occupant behaviour is one of the greatest sources of modelling error. Due to the COVID-19 pandemic in 2020, a natural experiment occurred where one can assume that there are no people present in the office building during this time period. This assumption reduces the number of parameters to investigate in the calibration process. The total internal heat gains estimated by Standard Norge (2020) are the same magnitude as the heat added by the radiators to the floors. Therefore it is evident that internal heat gains play a role in the indoor temperature (T_{air}) in the zone, and consequently also the radiator power as seen in Equations 3.1 and 3.2. In the results, it is clear that to keep the internal heat gains as predicted by Standard Norge (2020) in the model – but with no people and with equipment and lights at a minimum level – gives a more accurate indoor temperature during the experiment period whilst keeping the radiators calibrated. However, as the internal heat gains often are a source of error, these will also be considered for the sensitivity analysis in Chapter 5.4 for the modelled building during normal operation.

4.11.5 Loss in the Measurement Data

In the calibration process, the results from the model are compared to the measurement data which includes a loss of 10% from the measured power. The inclusion of said loss is deemed valid, as there can be many reasons for losses between the location of the measured power in the physical building and the radiators on each floor. One such reason is the assumptions presented in Chapter 3.3.1 and particularly Tables 3.1 and 3.2. The building can have a greater heat loss than what is modelled, which means that the radiators in

the model would increase the power and thus be more in line with the values from the measurements.

Moreover, Standard Norge (2014) estimated a distribution efficiency of 0,92-0,95 for hydronic heating systems and radiator efficiency of 0,87-0,90. These two efficiencies combined could account for a loss in the system in the magnitude of 10%. The radiators and the pipes in the hydronic heating system in the building in Oslo are located in the outer walls of the building. The impact of the outdoor temperature on the pipes and the radiators could also account for more losses between the connection to the district heating grid and the radiators which again would justify a reduction of 10% of the measurement data when comparing them to the results from the model.

The model assumes that the power measured at the location where the hydronic heating system is connected to the district heating grid is divided evenly between the seven floors which is covered by the radiator system. SINTEF has no data about the division of the total mass flow between the floors, but they do not assume that the various floors are supplied differently from the district heating central in the building. The basement could be an exception to this assumption as there are no data from this floor. However, the assumption of even distribution of the mass flow between the floors could be a source of error in the model.

4.11.6 The Zone

There are many parameters in the construction of the zone model that are based on estimated values from standards or similar buildings from the same time period. The internal walls and the level of furniture in the zones will impact the heat capacity in the room as observed by Hicham and Heiselberg (2017). The internal walls are added, but no furniture is added to the model. Depending on the level of furniture in the zones, the heat capacity could vary and thus impact the model's behaviour.

Another source of uncertainty in the zones is the buildings measurements. The floor plans in Appendix A are used to obtain the measurements for the building, however these are measured with a ruler off of the drawing which results in rounding errors. A better solution to this would be to have the exact dimensions of the building and its components. However, the data used to model the building gives a prediction of how the building with slightly different measurements behaves.

4.11.7 Indoor Temperature

Royapoor and Roskilly (2015) hypothesised that the HVAC category has the largest magnitude of error, as the temperature prediction in their model was more accurate whenever the AHU was idle. In the model for this Master's thesis, it is evident that the indoor air temperature is more sensitive to changes in the radiator power when comparing the model to the measured temperature from the building. This can be explained by the uncertainties when modelling HVAC systems, as many parameters are unknown. The modelled building is an older building, where most of the input data for the model is based off of rules

or regulations which were in effect during the time period when the building was built. However, some parameters were unknown such as which pipes were used in the hydronic heating system. This could cause an error to propagate throughout the system, resulting in an error. In the model for the thesis, it is observed that during the night time in the weekends after the 12th of March 2020 the model and the measured temperatures have a relatively constant deviation. Bontemps and Mora (2015) experienced a difference between the measured and simulated temperature of 5 °C, and Jorissen et al. (2019) obtained a difference of 2 K between the modelled building and measured data. The calibrated model has 70 instances where the difference between the average temperature in the building and the measured temperature is higher than 2 K and 0 instances where the differences between the temperatures are more than 5 °C. The results of the Master's thesis is within the same levels as the research.

Ascione et al. (2020) changed the heating schedules in order to calibrate the building by comparing the indoor air temperature from the simulation to the measured indoor air temperature. The results presented in Chapter 4.9.1 and 4.10.1 highlight the variations in the indoor temperatures in the model compared to the measurements during the experiment period. Comparing Figures 4.10, 4.11b and 4.11c, it can be seen that the indoor temperature in the model ("IG100_noppl") responds quicker to changes in the radiator power than the temperature in the physical building ("6_avg"). Moreover, the temperature in the physical building is more strongly correlated with the solar radiation. The model responds more to the changes in radiator due to the assumption that the air in the modelled zone is completely mixed. Yu et al. (2019) highlighted the benefits and disadvantages of the standard room model. The rapid response of the zone air temperature to changes in the radiator power is thus a consequence of the room model. The position of the temperature sensors in the measured zone is mostly in the south part of the building, which is also the part of the building that is most affected by the sun. It is therefore apparent in the average temperature of the floors that the sun plays an important role. The measured temperature in the building might thus be too reliant on the temperature on the South side of the building, as the actual average temperature might not be as dependent on the solar heat gain as depicted in the measured average temperature on the floors.

The modelled zone implements the standard room air model, and the heat added by the sun is therefore averaged over the entire zone's area resulting in a generally lower average temperature during the times of high solar gain to the building. Moreover, the local thermal comfort or discomfort as discussed by Georges et al. (2019) are not captured by the standard room model. The room model does not represent the airflows and the local thermal comfort as well as what is presented in the measured temperatures in the building.

Chapter 5

Application of Control Strategies

The second part of the Master's thesis focuses on applying control strategies to the calibrated model of the physical building to evaluate how the modelled building responds to different rule based control strategies. It would be ideal to use an MPC, but these are cumbersome to make and implement. Since implementing an MPC is outside of the scope for this thesis, this section will use RBCs instead.

5.1 Cases for Evaluation of Control Strategies

To evaluate how well the calibrated model operates during standard simulation conditions, different test cases are gathered. Common for all of them are the weather file, the model of the building and the internal heat gains used. The weather file is now the TMY weather file for Oslo, Fornebu. During a normal year of operation there will typically be people present during the whole year. Therefore, instead of removing the heat added by people after the 12th of March, the heat source is still present. There will be three cases and an overview of the parameters that vary between the cases are observed in Table 5.1.

Table 5.1: Overview of test cases.

	WCC	Night setback WCC	Pump settings
Case 1	Yes	Yes	100%
Case 2	Yes	No	100%
Case 3	Yes	No	Off at night/weekends

The first case investigates the control strategy, WCC with a 10 °C night and weekend setback of the WCC, that was used in the building during 2020. After the measurements were conducted in the spring of 2020, the building energy management system (BEMS) in the building was changed. Case 2 looks into the consequences of the new BEMS which

has a WCC, but no night and weekend setback. The final case considered for the thesis explores the possibility to turn off the pump in the heating central instead of implementing a night setback.

Moreover, it is important to ensure that the indoor temperatures are acceptable too. In order to obtain realistic values for the cases, the WCC is changed for Case 2 and 3. Keeping the WCC with no night setback results in unnecessary heating during the night and weekends, so a method to solve this is to lower the supply temperature of the WCC at design outdoor temperature. It is the opposite for Case 3, where the supply temperature of the WCC is increased to ensure that the pumps can supply the required water to the radiators to maintain an acceptable indoor air temperature. An overview of the adjustments is presented below.

1. Reduce the WCC to 60 °C at -10 °C outside for Case 2 in order to reduce the supply temperature.
2. Increase WCC to 80 °C at -5 °C outside for Case 3 in order to increase the supply temperature to the building.

5.2 Results of the Control Strategies

The control strategies explained in Chapter 5.1 are applied to the calibrated model, and compared in terms of energy use and indoor air temperature.

5.2.1 Radiator Power

Figure 5.1 presents the relationship between the radiator power and the temperature difference between the radiator and the zone for the three cases mentioned in Chapter 5.1.

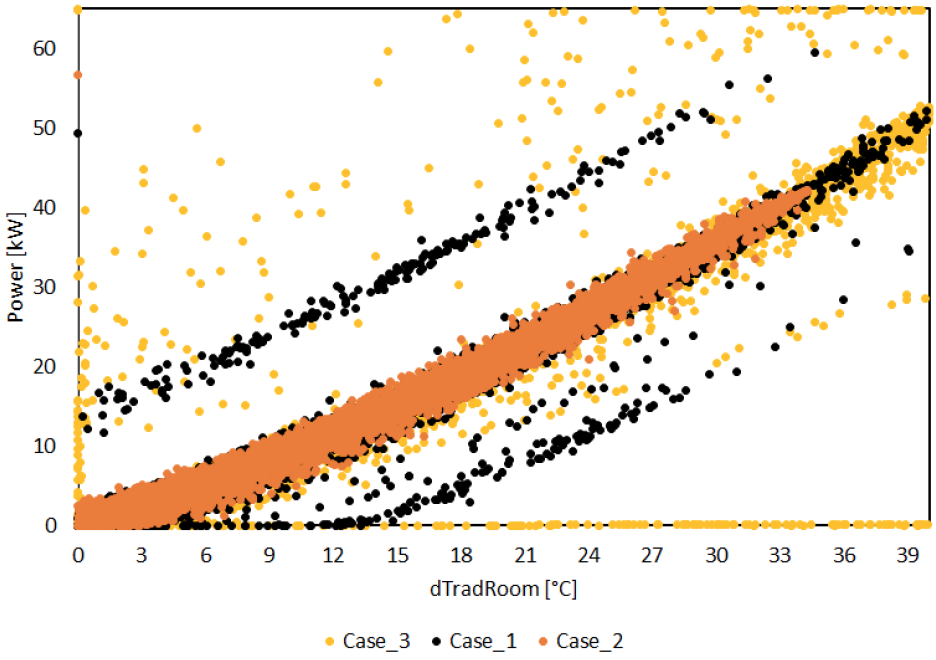

Figure 5.1: Comparison between the supplied radiator power and the temperature difference between the radiator and the room for the different cases.

In Figure 5.1 it is easily observed that Case 2 has no night setback as all of its results are within the same range. The night setback in Case 1 can be observed by the two distinct lines above and below the main results. For Case 3 it is observed that it has some extreme points outside of the trajectory in the middle section of Figure 5.1. These extreme points are due to the pump turning on and off during the morning and night. The pump then needs to add extra power to get the radiator power up to a level where it provides the necessary heat to the zones.

5.2.2 Energy Use

The energy use in the modelled building is presented in Table 5.2. The energy use is calculated by the component called ”EnergyDiffCalc”, as seen in Figure 3.6.

Table 5.2: Overview of the results from the test cases.

	West [kWh]	East [kWh]	Total [kWh]	Specific [kWh/m^2]
Case 1	61 100	43 650	104 750	48,4
Case 2	75 100	53 650	128 750	59,4
Case 3	58 450	41 750	100 200	46,3
Measurements	-	-	167 000	44,0

The case labelled ”Measurements” in Table 5.2 is measured by Walnum (2020) in the building in 2017. During the measurement period the WCC was active and there was also a night setback. The area considered for the modelled building is smaller than the area for the measurements, which explains the large deviation for the total energy use. Case 2 which has no night and weekend setback is the case that separates itself from the other cases in Table 5.2. It performs poorly with an increase of 13,1 kWh/m^2 (28,3% increase) in specific energy use compared to Case 3. Furthermore, the energy supplied by the radiators is also compared to the supply temperature of the radiators in the different cases, and the relationship is presented in Figure 5.2.

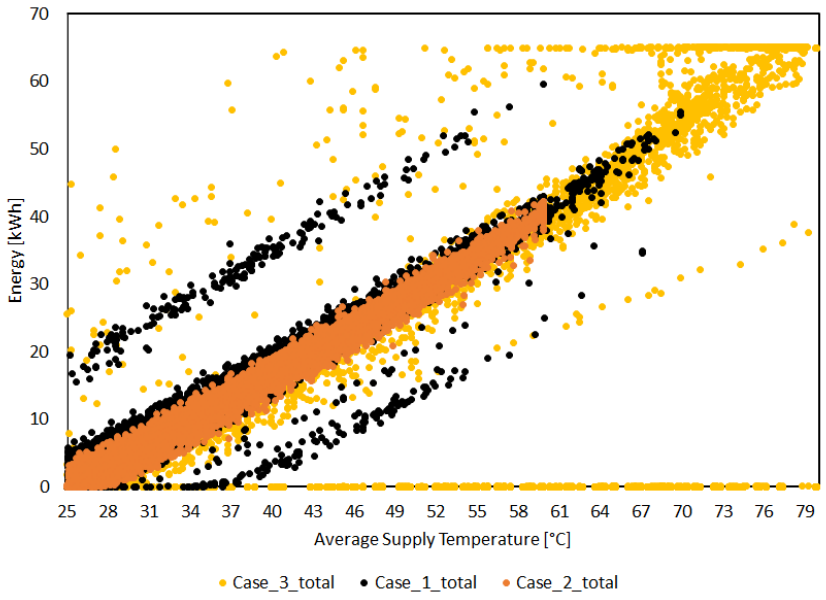

Figure 5.2: Total energy supplied by the radiators per hour and the average supply temperature.

The West and East circuits for the cases are added together in Figure 5.2, and plotted against the average supply temperature. All of the cases have the same tendency in Figure 5.2. However, Case 1 has the night setback which results in the two parallel lines for both the West and East circuit due to the start and stop of the night setback. Case 3 has generally a higher energy use for the same supply temperatures as the other cases for both of the circuits. Moreover, Case 3 has the night setback of the pumps, which results in the high and low outliers in Figure 5.2. It can be observed in Case 3 that the radiators reach their maximum power output, resulting in the horizontal line to the top right.

The radiator supply temperature is also dependent on the ambient temperature. A comparison of the radiator supply temperature and the ambient temperature is presented in Figure 5.3.

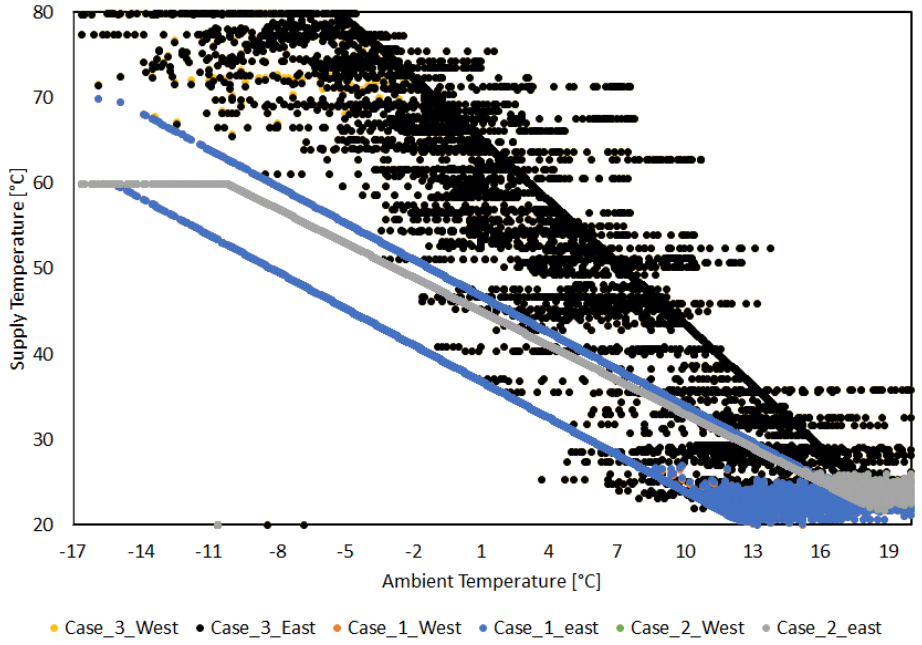

Figure 5.3: Relationship between the supply temperature to the radiators and the ambient temperature in the cases.

Case 1 is the only case with a night setback on the WCC in Figure 5.3. The night setback on the WCC for Case 1 is evident in the two distinct linear blue lines, and as both the West and East circuit for Case 1 have the same WCC, they perfectly overlap in Figure 5.3. For Case 2 it is clear that there is no night setback as there is only one line in Figure 5.3 where the East and West circuits overlap. The lowered WCC for Case 2 (60 °C at -10 °C outside) is observed by the horizontal section of the graph before it reaches -10 °C ambient temperature. Lastly, the night setback in Case 3 is independent of the ambient temperature as it only follows a time schedule for the pumps. Both the West and East circuit for Case

3 which has a night setback on the pumps overlap with each other, as they are modelled in the same manner. In Figure 5.3 one observes the same linear relationship for Case 3, albeit not so clear as for the other two cases. It is also observed that the WCC is shifted higher than the other two cases, with a supply temperature of 80 °C at -5 °C.

Lastly the comparison between the cases and their relationship between the energy consumption and the ambient temperature is presented in Figure 5.4. The West and East circuits for each of the cases are added together in Figure 5.4.

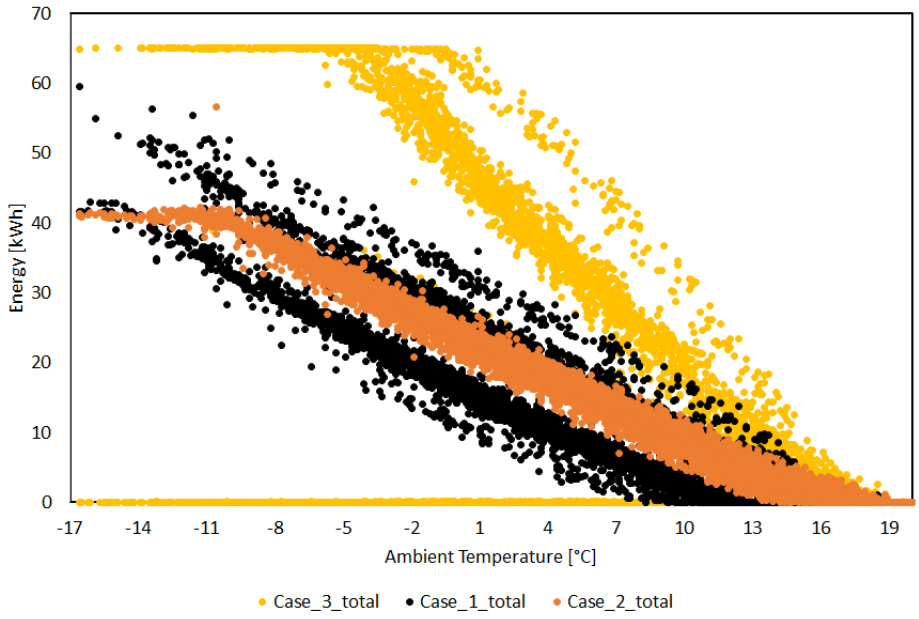

Figure 5.4: Relationship between the energy consumption and the ambient temperature in the cases.

Case 3 West circuit has the highest energy consumption for a given ambient temperature in Figure 5.4 due to the increased WCC, but this is also the case where the radiators have to supply more energy the moment when the pumps' night setback is not longer active. Case 1 has two distinct lines which indicate the night setback and normal operations. Lastly, as Case 2 has no night setback one easily observes that the energy supplied to the building only depends on the ambient temperature.

5.2.3 Load Duration Curves for the Control Strategies

Table 5.2 indicates that there are differences in the total energy use of the different control strategies. To highlight the effect of the different controls of the heating strategies, the differences in energy use between the control strategies in the modelled building are presented by load duration curves in Figure 5.5.

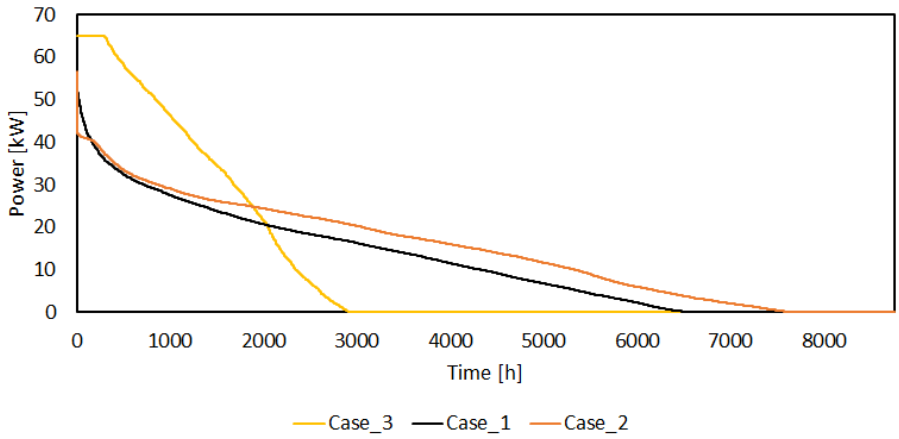

Figure 5.5: Load duration curves for the different control strategies.

From Table 5.2, the energy use between the cases is somewhat similar. Inspecting Figure 5.5 it can be seen that Case 3 has significantly more hours with high power output and also many more hours with no power output. This shows that Case 3 – the case with night and weekend setback of the pumps – features both higher intensity and variation for the components, with many starts and stops. This may lead to a more rapid component degradation. Cases 1 and 2 have a more stable operating scheme.

5.2.4 Indoor Air Temperature

The indoor air temperature should be within acceptable levels for the different cases presented in Chapter 5.1 to be viable solutions. For comparison between the cases, it is assumed that the average indoor air temperature of the floors represent the indoor air temperature in the building. Table 5.3 illustrates how many hours are below 19 °C during work hours for the different cases. The work hours are assumed to be from 06.00 to 18.00, Monday to Friday. Holidays are not considered. It is the average temperature of the second to the seventh floor that is considered for the comparison.

Table 5.3: Overview of discomfort hours.

	< 19 °C	< 21 °C
Case 1	5	1044
Case 2	0	147
Case 3	187	936

It is evident in Table 5.3 that Case 3 has significant number of hours below 19 °C, which is below the recommended levels of Arbeidstilsynet (2021). For Case 1 and 2 which have

longer hours of duration, as seen in Figure 5.5, the indoor temperature is rarely or never below the legal limit. Case 1 and 3 have a significant number of hours below 21 °C, whereas Case 2 with no night setback achieves the fewest number of work hours below 21 °C.

5.3 Evaluation and Analysis of the Control Strategies

5.3.1 Energy Use

The three cases considered for the building during normal operations in Chapter 5.2.2 illuminate differences between the various control strategies in terms of energy use. Case 3, where there is no pumps at night and in the weekend, has the lowest specific energy use of all the cases in Table 5.2. However, Figure 5.5 highlights the drawback of this control strategy and its limited operating hours. The night and weekend setback of the pumps forces the hydronic heating system to emit more heat during the hours of operation compared to the other cases. The benefit of the strategy is the reduced use of energy during hours when there are no people present in the building, but this comes at a price - the indoor temperature as seen in Table 5.3.

Moreover, Case 2 which has no night setback has the highest specific energy use of all the evaluated control strategies in Table 5.2 and the fewest hours below both 19 and 21 °C as seen in Table 5.3. The question to ask now is whether it is actually necessary to use this much energy to maintain a satisfactory indoor air temperature. A modified version of this control could be to introduce a weekend setback. The weekend setback would ensure that the building is still heated during the nights in the work week, but it would reduce the energy use during weekends when it can be assumed that there are no people present.

The control strategy consisting of a WCC and a night and weekend setback, Case 1, lies in the middle of Case 2 and 3 in terms of both specific energy use in Table 5.2 and WCC set point as seen in Figure 5.3. The results in Chapter 5.2.2 indicate that out of the three solutions, Case 1 results in the lowest energy use in the building whilst still maintaining the indoor air temperature to a great extent.

5.3.2 Indoor Air Temperature

The indoor air temperature experienced in the building due to the control strategies varied between the different strategies. The main idea is to have a satisfactory indoor air temperature whenever people are present. If instead of the proposed time of checking from 06.00-18.00, one investigates the time interval from 07.00-17.00 which is according to Figure 3.2. Table 5.4 presents these results and investigates the percentage change to the results in Table 5.3.

The results from Table 5.4 indicate that the problem area for the modelled building is the morning. Another trend that presented itself in the indoor air temperature results is that Mondays are generally the problem. For the case with a WCC and a night setback (Case

Table 5.4: Comparison of discomfort hours between longer and shorter work hours.

	Long: 06.00-18.00		Short: 07.00-17.00		Difference	
	< 19 °C	< 21 °C	< 19 °C	< 21 °C	< 19 °C [%]	< 21 °C [%]
Case 1	5	1044	2	859	-60	-18
Case 2	0	147	0	107	0	-27
Case 3	187	936	143	770	-24	-18

1), 5 out of 5 hours under 19 °C are on Mondays. For Case 3, where the pumps turn off at night, 124 out of 187 hours under 19 °C are during Mondays. Therefore, a different night setback schedule for the pumps (Case 3) that has an earlier start time, or no weekend setback, might provide better indoor air temperature results. This could help reach the minimum levels set by Arbeidstilsynet (2021).

Another reason for the cold indoor temperatures in the modelled building can be the difference in the outdoor temperature for the two weather files used in this thesis. Figure 5.6 presents the variations in the outdoor temperature at Blindern in 2020 and Fornebu in a TMY.

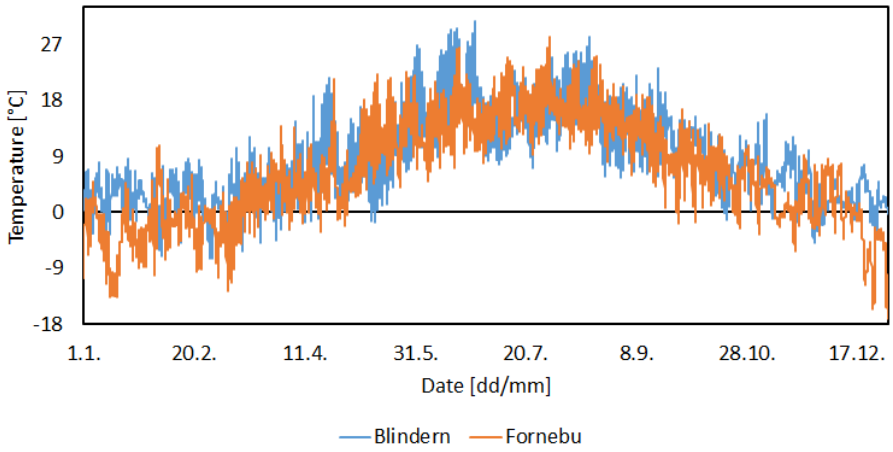

Figure 5.6: Difference in the outdoor temperature between the TMY file and the weather in 2020.

There are 8760 entries in Figure 5.6, one for each hour in a year, and in 5707 of these hours did the TMY file have a lower outdoor temperature than the weather in 2020. de Wilde (2014) argued that the performance gap between the measured and simulated values are wider in colder years. Figure 5.6 can be an example of colder weather resulting in poorer performance for the modelled building.

5.3.3 The Weather Compensated Curves

The WCC supply temperature at different outdoor temperatures for the various cases presented in Table 5.1 are found by means of trial and error and ensuring that the temperatures in the building are seemingly acceptable. Therefore, the chosen WCC setpoints might not be realistic. Moreover, there is some uncertainty about how many degrees the night setback subtracts from the WCC. The assumption of 10 °C is based on observations from the measurement data during the spring of 2020, however it could be different. A lower night setback will result in a lower energy consumption over the whole year. The degrees for the night setback of the WCC are investigated in the sensitivity analysis in Chapter 5.4.

5.3.4 MPC Possibility

Serale et al. (2018) argue that commercial buildings justify the investment cost of implementing MPCs as the cost reduction potential outweighs the investment needed. The office building modelled for this case is within the aforementioned category that could argue for an investment in MPCs. Kavgic et al. (2015) argue that high thermal mass is vital and occupancy of twelve hours or less during the day is optimal for buildings where MPCs can be implemented. The case building in Oslo is a concrete building, meaning that it has a high thermal mass, and is an office space, resulting in occupancy of less than twelve hours a day. The authors also concluded that medium and large offices have the characteristics that are favourable to MPC.

Given the above considerations, it seems appropriate to investigate the effect of an MPC on the SINTEF Community building. However, this is outside the scope of this work and therefore only RBCs have been investigated. The energy use in the building with the different RBCs varies greatly. However, Aste et al. (2017) indicate that the implementation of advanced control strategies such as MPC can reduce the energy consumption in a building by 15 - 30 % compared to RBC. The results are reaffirmed by Jorissen and Helsen (2019) which obtained a 12,8 % reduction by using MPC instead of RBC. Lastly, when comparing WCC and MPC in an ideal setting and at a constant price signal Walnum et al. (2020) found that the MPC had a 12 % reduction in energy cost and energy consumption. This research highlights the potential in terms of reduction in energy use in the modelled building if the MPC is implemented instead of any of the mentioned RBCs in Chapter 5.1.

5.4 Sensitivity Analysis of the Modelled Building

Reddy (2006) argued that a sensitivity analysis should be performed to identify parameters for the calibration process. However, it is also worthwhile to investigate how sensitive the final model is to the assumptions used in the calibrated model. From the specialization project, it was predicted that internal gains and the schedule of the blinds needed to be updated for the model in the Master's thesis. The final model for the Master's thesis was calibrated with internal gains of 100 % of the standard values as presented in Standard Norge (2020) and with blinds 50% down at all times. Moreover, due to the aforementioned uncertainty of the night setback for the WCC, it is decided to investigate the effects of this too. A sensitivity analysis of these parameters is therefore undertaken to address how the estimates of the internal heat gains, the temperature of the night setback on the WCC and the blinds will impact the energy use in the modelled building during normal operations. Table 5.5 presents the various cases for the sensitivity analysis. The case considered for the sensitivity analysis is Case 1 with WCC and night setback as presented in Table 5.1.

Table 5.5: Overview of the cases for the sensitivity analysis.

	Blinds [%]	IG [% of Standard Norge (2020)]	Night Setback Case 1 [°C]
Original	50	100	10
Blinds 25	25	100	10
Blinds 75	75	100	10
IG 80	50	80	10
WCC 15	50	100	15

The results of the various cases in Table 5.5 are presented in Figure 5.7.

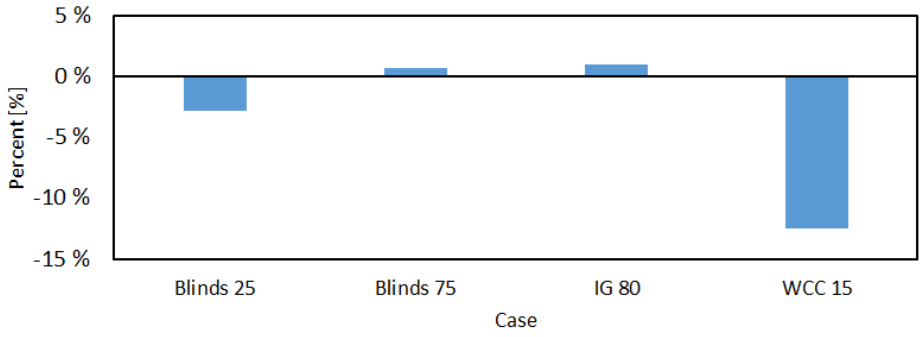

Figure 5.7: Percent difference in the total energy use for the cases in the sensitivity analysis.

The results from Figure 5.7 clearly highlight the energy saving potential in having a night setback on the WCC, which is in line with the results in Table 5.2. The change in the temperature of the WCC has the biggest impact on the energy use in the building, which was also indicated in Table 5.2. In Table 5.2 it is observed that removing the night setback altogether on the WCC increases the energy use in the building considerably. Therefore, a hypothesis is that the opposite should also be true, which is confirmed in Figure 5.7. However, the results from Figure 5.7 need to be evaluated against the hours below comfortable temperature levels. Table 5.6 presents the number of hours for the cases investigated in the sensitivity analysis.

Table 5.6: Overview of discomfort hours for the sensitivity analysis.

	< 19 °C	< 21 °C
Original	5	1044
Blinds 25	4	832
Blinds 75	4	1093
WCC15	63	1597
IG 80	40	1029

In Table 5.6 it is observed that the lowered night setback for the WCC increases the number of discomfort hours under 19 °C and under 21 °C significantly. Therefore, in order to implement the lower WCC at night and weekends, the schedule for when the setback is initiated needs to be updated to ensure that the hours below the requirements are reduced.

Moreover, the hypothesis that the internal heat gains impact the energy use in the building to a large degree is not evident in the results in Figure 5.7. However, in Table 5.6 it is clear that the number of hours below 19 °C increases for this scenario. As a result of this, it is highlighted that variations in the internal heat gains in the modelled building do impact the energy use, but more importantly, they influence the thermal comfort of people in the building.

Lastly, blinds impact the energy use in the building, with a 3 % reduction for the ”Blinds 25” case and an increase of 0,7 % for the ”Blinds 75” case as seen in Figure 5.7. Furthermore, the hours below 21 °C improve for the scenario where the blinds 25 scenario, and the number of hours below 21 °C for the Blinds 75 case increase. It is therefore important to consider the blinds for the modelled building as they impact the thermal comfort in the building, but not the energy use to a great extent.

Chapter 6

Conclusion and Further Work

6.1 Conclusion

The aim of this Master's thesis was to create an emulator of SINTEF's office in Oslo to test and compare different control algorithms, such as MPCs. The model should be developed in the Dymola/Modelica environment. The first step was to create a calibrated model of the office building, and the second step of the thesis was to apply different rule based control strategies to the calibrated building and evaluate them.

The modelled building for the calibration process used input data from measurements of the building in Oslo, in order to reduce the number of parameters for calibration. By investigating the response of the indoor temperature in the modelled building during a PRBS experiment during the Easter of 2020, the nominal power of the hydronic heating system and internal gains in the building ensured that the model was calibrated.

The calibrated model was then used to evaluate different control strategies. The literature suggests that MPCs outperform RBCs in terms of energy use, and ideally an MPC would be used in this work. MPCs are cumbersome to implement and this is outside the scope of this thesis. Instead, three different RBCs were used to test the calibrated model under normal operating conditions. All of the controls had a WCC. One also had a night setback, the second did not have a night setback and the third control turned the pumps in the hydronic heating system off at night. The results of the different control strategies presented the energy use and indoor air temperatures of the different cases. The case where the pumps are turned off at night generally struggle to heat the building sufficiently by Monday morning, whereas the case with no night setback had a more satisfactory indoor air temperature. The case with a WCC and a night setback had a more favourable energy use compared to the case with no night setback and could ensure that the indoor temperature was more realistic than the case where the pumps are turned off.

Lastly, a sensitivity analysis of the modelled building was conducted to investigate the

influence of certain parameters to the energy use and thermal comfort in the modelled building. The significance of the level of blinds or the internal heat gain were small. However a night setback of 15 °C, as compared to 10 °C, reduced the energy use in the case with a WCC and night setback by 12 %. These measures need to be considered together with their impact on the indoor air temperature in the modelled building. The results of the sensitivity analysis highlighted the need to update the setback schedule for the case with a WCC of -15 °C in the weekends for it to be a better solution.

6.2 Further Work

The model for the Master's thesis used assumptions from standards to implement the heat added from internal gains. The values from the standards might not be accurate for this particular building, and the time period of measurements turned out to be during a pandemic resulting in different internal heat gains in the building than during normal operating hours. However, the internal heat gains for a typical day in the office building can be stipulated by more discussions with people working in the building. Moreover, measurements of the heat added by machines and lights for this particular building can be conducted to obtain more accurate input.

Moreover, the district heating substation in the building is simplified in the model of the entire building. The substation is ideal, and can be modelled in a more realistic manner. By implementing an improved connection to the district heating grid, the response by the modelled building will likely correspond more to the physical building.

The results from the different control strategies in Chapter 5.2.2 illustrate the need to conduct more research to find an optimal control strategy for the building. The calibration process conducted for the modelled building corresponds to the measurements of the building and to the model with WCC and night setback (Case 1). However, an interesting area for more research is to find more optimal control strategies that could reduce the energy consumption in the building. The results in the Master's thesis indicated the possibility of reducing the energy use in the building by changing the RBC. A different control strategy can be MPCs. These may be better able to lower the energy use in the buildings, or they can have improved performance with different objective functions such as higher thermal comfort or lower energy cost. This control was not tested for the Master's thesis and is a natural focus for further research.

Bibliography

Afram, A., Janabi-Sharifi, F., 2014. Theory and applications of HVAC control systems – A review of model predictive control (MPC). Building and Environment 72, 343–355.

Arbeids- og sosialdepartementet, 2020. Arbeidsplassforskriften. https://www.arbeidstilsynet.no/regelverk/forskrifter/arbeidsplassforskriften/2/2-8/ [Accessed: 12.03.21].

Arbeidstilsynet, 2021. Temperatur - varme og kulde på jobben. https://www.arbeidstilsynet.no/tema/temperatur/ [Accessed: 07.06.21].

Ascione, F., Bianco, N., Iovane, T., Mauro, G., Napolitano, D., Ruggiano, A., Viscido, L., 2020. A real industrial building: Modeling, calibration and Pareto optimization of energy retrofit. Journal of Building Engineering 29.

Aste, N., Manfren, M., Marenzi, G., 2017. Building Automation and Control Systems and performance optimization: a framework for analysis. Renewable and Sustainable Energy Reveiws 75, 313–330.

Behrendt, M., 2009. Own work, cc by-sa 3.0. https://commons.wikimedia.org/w/index.php?curid=7963069 [Accessed: 11.12.20].

Blum, D., Jorissen, F., Huang, S., Arroyo, J., Benne, K., Li, Y., Gavan, V., Rivalin, L., Helsen, L., Vrabie, D., Wetter, M., Sofos, M., 2019. Prototyping the BOPTEST Framework for Simulation-Based Testing of Advanced Control Strategies in Buildings, Rome, Italy.

Bontemps, S., Mora, L., 2015. Holzkirchen house modelling using Modelica Buildings library and comparison with measurements, Hyderabad, India.

Brattebø, H., O'Born, R.J., Sartori, I., Klinski, M., Nørstebø, B., 2014. Typologier for norske boligbygg - Eksempler på tiltak for energieffektivisering .

Drgoňa, J., Arroyo, J., Cupeiro Figueroa, I., Blum, D., Arendt, K., Kim, D., Ollé, E.P., Oravec, J., Wetter, M., Vrabie, D.L., Helsen, L., 2020. All you need to know about model predictive control for buildings . Annual Reviews in Control 50, 190–232.

Duffie, J.A., Beckman, W., 2013. Solar Engineering of Thermal Processes. John Wiley & Sons, Inc., Hoboken, USA.

Erbs, D., Klein, S., Duffie, J., 1982. Estimation of the diffuse radiation fraction for hourly, daily and monthly-average global radiation. Solar Energy 28, 293–302.

European Parliament, 2010. DIRECTIVE 2010/30/EU OF THE EUROPEAN PARLIAMENT AND OF THE COUNCIL of 19 May 2010 on the indication by labelling and standard product information of the consumption of energy and other resources by energy-related products (recast). Official Journal of the European Union 53.

Fortum Oslo Varme, 2018. Bestemmelser om tilknytning til fortum oslo varmes fjernvarmenett for eksisterende bygg. https://www.fortum.no/sites/default/files/documents/bestemmelser_om_tilknytning_til_fjernvarmeanlegget_eksisterende.pdf [Accessed: 19.10.20].

Geberit International Sales AG, 2021. Geberit mapress stainless steel system pipe, crnimo, small bundle. https://catalog.international.geberit.com/en-NT/Geberit-Mapress-Stainless-Steel-system-pipe,-CrNiMo,-small-bundle/OVE_502637.html [Accessed: 26.05.21].

Georges, L., Thalfeldt, M., Skreiberg, O., Fornari, W., 2019. Validation of a transient zonal model to predict the detailed indoor thermal environment: Case of electric radiators and wood stoves. Building and Environment 149, 169–181.

González, D.F., Yebra, L.J., 2015. Comparison case between Modelica and specialized tools for building modelling, Vienna Austria.

Gundersen, M.W., 2020. Modelica emulator for MPC applications in buildings. Specialization project .

Hensen, J.L.M., Lamberts, R., 2011. Building Performance Simulation for Design and Operation. Spon Press.

Hicham, J., Heiselberg, P., 2017. Influence of internal thermal mass on the indoor thermal dynamics and integration of phase change materials in furniture for building energy storage: A review. Renewable and Sustainable Energy Reviews 69, 19–32.

Hofstad, K., 2020. solenergi. https://snl.no/solenergi [Accessed: 02.03.21].

Holmgren, W., Calama-Consulting, Hansen, C., Mikofski, M., Anderson, K., Lorenzo, T., Krien, U., bmu, Stark, C., DaCoEx, Driesse, A., konstant_t, mayudong, Peque, M., Heliolytics, Miller, E., Anoma, M.A., Guo, V., Boeman, L., jforbess, Lunel, T., Morgan, A., Stein, J., Leroy, C., R, A.M., JPalakapillyKWH, Dollinger, J., Anderson, K., MLEEFS, Dowson, O., 2021. pvlib/pvlib-python: v0.8.1. https://doi.org/10.5281/zenodo.4417742 [Accessed: 04.03.21].

Holmgren, W.F., Hansen, C.W., Mikofski, M.A., 2018. PVlib python: a python package for modeling solar energy systems. The Journal of Open Source Software 3, 884.

Jones, R.V., Fuertes, A., de Wilde, P., 2015. The gap between simulated and measured energy performance: A case study across six identical new-build flats in the UK, Hyderabad, India.

Jorissen, F., Boydens, W., Helsen, L., 2019. Model implementation and verification of the envelope, HVAC and controller of an office building in Modelica. Journal of Building Performance Simulation 12, 445–464.

Jorissen, F., Helsen, L., 2019. Integrated Modelica Model and Model Predictive Control of a Terraced House Using IDEAS, Regensburg, Germany.

Kauko, H., Kvalsvik, K.H., Rohde, D., Nord, N., Utne, A., 2018. Dynamic modeling of local district heating grids with prosumers: A case study for Norway. Energy 151, 261–271.

Kavgic, M., Hilliard, T., Swan, L., 2015. Opportunities for implementation of MPC in commercial buildings. Energy Procedia 78, 2148–2153.

Kleissl, J., 2013. Solar Energy Forecasting and Resource Assessment. Academic Press, Oxford, UK.

Kotireddy, R., Loonen, R., Hoes, P.J., Hensen, J.L.M., 2019. Building performance robustness assessment: Comparative study and demonstration using scenario analysis. Energy and Buildings 202.

Lauster, M., Remmen, P., Fuchs, M., Teichmann, J., Streblow, R., Müller, D., 2014. Modelling long-wave radiation heat exchange for thermal network building simulations at urban scale using Modelica, Lund, Sweden.

Lawrence Berkeley National Laboratory, 2020. Buildings.thermalzones.reducedorder.rc.fourelements. https://simulationresearch.lbl.gov/modelica/releases/v4.0.0/help/Buildings_ThermalZones_ReducedOrder_RC.html#Buildings.ThermalZones.ReducedOrder.RC.FourElements [Accessed: 27.10.20].

Lawrence Berkeley National Laboratory, 2021. Buildings.fluid.heatexchangers.radiators. https://simulationresearch.lbl.gov/modelica/releases/v3.0.0/help/Buildings_Fluid_HeatExchangers_Radiators.html [Accessed: 21.05.21].

Mahdavi, A., 2020. In the matter of simulation and buildings: some critical reflections. Journal of Building Performance Simulation 13, 26–33.

Norconsult, 2013. Veileder 5/2013. praktisk veileder for energimerking. http://publikasjoner.nve.no/veileder/2013/veileder2013_05.pdf [Accessed: 08.10.20].

Norsk Klimaservicesenter, 2021. Observasjoner og værstatistikk. https://seklima.met.no/observations/ [Accessed: 23.02.21].

OpenModelica, 2021. Buildings.boundaryconditions.weatherdata.readertmy3. https://build.openmodelica.org/Documentation/Buildings.BoundaryConditions.WeatherData.ReaderTMY3.html [Accessed: 30.04.21].

Perez, R., Ineichen, P., Moore, K., Kmiecik, M., Chain, C., George, R., Vignola, F., 2002. A new operational model for satellite-derived irradiances: Description and validation. Solar Energy 73, 307–317.

Pilkington Floatglas AB, 2017. Glassfakta. https://www.pilkington.com/-/media/pilkington/site-content/norway/glassfakta2017_18_no.pdf [Accessed: 28.10.20].

Prívara, S., Široký, J., Ferkl, L., Cigler, J., 2011. Model predictive control of a building heating system: The first experience. Energy and Buildings 43, 564–572.

Purmo Group AS, 2019. Compact [c]. https://www.purmo.com/no/produkter/radiatorer-for-vannbasert-varme/stalpanelradiatorer/purmo-compact.htm#tab-nedlastinger [Accessed: 04.12.20].

Reda, I., Andreas, A., 2004. Solar Position Algorithm for Solar Radiation Applications. Technical Report. National Renewable Energy Laboratory.

Reddy, T., 2006. Literature review on calibration of building energy simulation programs: Uses, problems, procedure, uncertainty, and tools. ASHRAE Transactions 112, 226–240.

Reno, M.J., Hansen, C.W., Stein, J.S., 2012. Global Horizontal Irradiance Clear Sky Models: Implementation and Analysis. Technical Report. Sandia National Laboratories.

Rognan, L.M.H., 2018. Photovoltaic Power Prediction and Control Strategies of the Local Storage Unit at Campus Evenstad. Master's thesis.

Rossing, N.K., Storli, P., Völler, S., Fagerli, T., 2020. Fornybar energi. NTNU Grafisk senter, Trondheim, Norway. chapter 2. p. 10.

Royapoor, M., Roskilly, T., 2015. Building model calibration using energy and environmental data. Energy And Buildings 94, 109–120.

RWTH Aachen University, 2017. Teaser 0.6.0 documentation. http://rwth-ebc.github.io/TEASER/ [Accessed: 27.10.20].

Serale, G., Fiorentini, M., Capozzoli, A., Bernardini, D., Bemporad, A., 2018. Model Predictive Control (MPC) for Enhancing Building and HVAC System Energy Efficiency: Problem Formulation, Applications and Opportunities. Energies 11, 631.

SINTEF, 2015. 524.213, innervegger med trestendere. https://www.byggforsk.no/dokument/373/524213_innervegger_med_trestendere [Accessed: 10.11.20].

SINTEF, 2016. 733.161. eldre vinduer. vindusformer og materialer. https://www.byggforsk.no/dokument/701/eldre_vinduer_vindusformer_og_materialer#i81 [Accessed: 28.10.20].

SINTEF, 2018. 451.021, klimadata for termisk dimensjonering og frostsikring. https://www.byggforsk.no/dokument/204/klimadata_for_termisk_dimensjonering_og_frostsikring [Accessed: 27.10.20].

Solmaz, A., 2019. A critical review on building performance simulation tools. Alam cipta 12, 7–21.

Standard Norge, 2014. NS 3031:2014, Beregning av bygningers energiytelse. Metode og data .

Standard Norge, 2020. SN-NSPEK 3031:2020, Bygningers energiytelse. Beregning av energibehov og energiforsyning .

The American Society of Heating, Refrigerating and Air-Conditioning Engineers, 2014. ASHRAE Guideline 14-2014 - Measurement of Energy, Demand, and Water Savings .

The European Commission, 2020. Energy performance of buildings directive. https://ec.europa.eu/energy/topics/energy-efficiency/energy-efficient-buildings/energy-performance-buildings-directive_en#facts-and-figures [Accessed: 02.11.20].

U.S. Department of Energy Federal Energy Management Program, 2015. M&V Guidelines: Measurement and Verification for Performance-Based Contracts Version 4.0 .

Walnum, H.T., 2020. Memo MPC for Børrestuveien 3.

Walnum, H.T., Sartori, I., Bagle, M., 2020. Model predictive control of District Heating substations for flexible heating of buildings, Oslo, Norway.

Wetter, M., Bonvini, M., Nouidui, T.S., 2016. Equation-based languages – A new paradigm for building energy modeling, simulation and optimization. Building Research and Information 117, 290–300.

Wetter, M., et al., 2015. IEA EBC Annex 60 Modelica library – an international collaboration to develop a free open-source model library for buildings and community energy systems, Hyderabad, India.

de Wilde, P., 2014. The gap between predicted and measured energy performance of buildings: A framework for investigation. Automation in Construction 41, 40–49.

Williamson, T.J., 2010. Predicting Building Performance: The ethics of computer simulation. Building Research and Information 38, 401–410.

Yu, Y., Megri, A.C., Jiang, S., 2019. A review of the development of airflow models used in building load calculation and energy simulation. Building Simulation 12, 347–363.

Zijdemans, D., 2012. Vannbaserte oppvarmings- og kjølesystemer. Skarland Press AS.

Appendix A

Assumptions for Modelling the Building

Table A.1: The build-up of building elements.

Element	Material	Width [m]	Thermal Conductivity [W/mK]	Density [kg/m^3]	Specific Heat Capacity [J/kgK]
External Wall	Brick clay	0,108	0,40	1036	1000
	Mineral wool	0,075	0,04	60	850
	Concrete	0,050	2,10	2420	1000
Internal Wall	Gypsum	0,13	0,30	850	1000
	Mineral wool	0,06	0,04	60	850
	Gypsum	0,13	0,30	850	1000
Floor	Concrete	0,10	2,10	2420	1000
	Wood wool	0,12	0,081	390	2000
	Concrete	0,10	2,10	2420	1000
Roof	Concrete	0,10	2,10	2420	1000
	Mineral wool	0,10	0,04	60	850
	Concrete	0,10	2,10	2420	1000

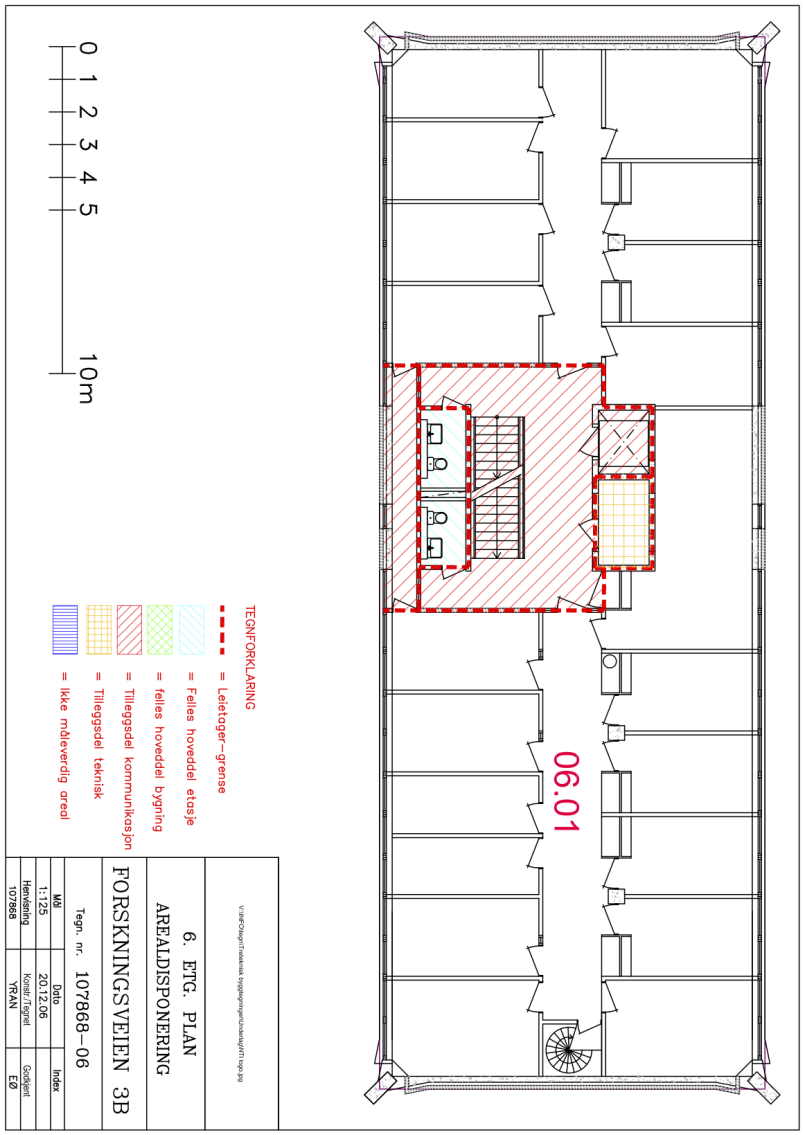

Figure A.1: Overview of the 6th floor.

Table A.2: Overview of internal walls and number of radiators in each floor.

Floor	Internal walls [m^2]	Number of radiators	Nominal power per radiator [W]
U	203,40	7	1281
2	654,75	15	569
3	812,70	18	498
4	793,80	19	498
5	565,00	11	783
6	926,10	20	427
7	817,09	18	498

Table A.3: Modelling the duct system.

Floor	Volumetric flow rate [m^3/h]	Velocity [m/s]	Diameter [m]	Duct size [mm]	Pressure change [Pa]
AHU - 7	15163,75	5	1,051	1000	3,5
7 - 6	12949,56	5	0,971	1000	3,5
6 - 5	10735,38	5	0,884	1000	3,5
5 - 4	8521,19	5	0,788	800	3,5
4 - 3	6307,00	5	0,678	800	3,5
3 - 2	4092,81	5	0,546	630	3,5
2 - U	2296,00	5	0,409	500	3,5
7	2215,00	5	0,402	500	71,0
6	2215,00	5	0,402	500	67,5
5	2215,00	5	0,402	500	64,0
4	2215,00	5	0,402	500	60,5
3	2215,00	5	0,402	500	57,0
2	1797,00	5	0,362	400	53,5
U	2296,00	5	0,409	500	50,0

Table A.4: Modelling the pipe system.

Floor	Pressure change [Pa]	Velocity [m/s]	Diameter [mm]
Central - U	350	0,92	54
U - 2	350	0,79	54
2 - 3	350	0,66	54
3 - 4	350	0,53	54
4 - 5	350	0,68	42
5 - 6	350	0,67	35
6 - 7	350	0,52	28
7	0	-	28
6	700	-	28
5	540	-	28
4	1050	-	28
3	1400	-	28
2	1750	-	28
U	2100	-	28

Appendix B

Validation of Meteorological Data

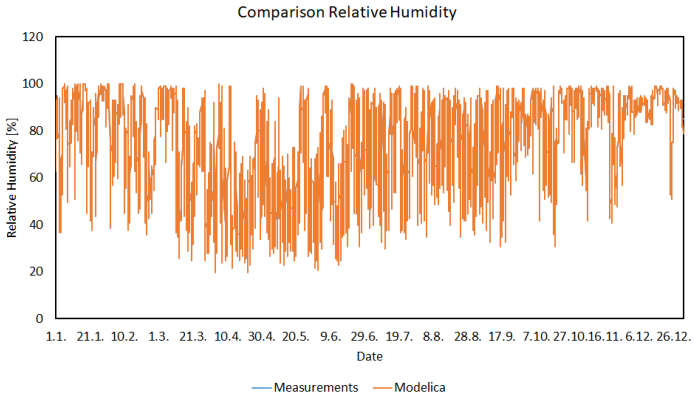

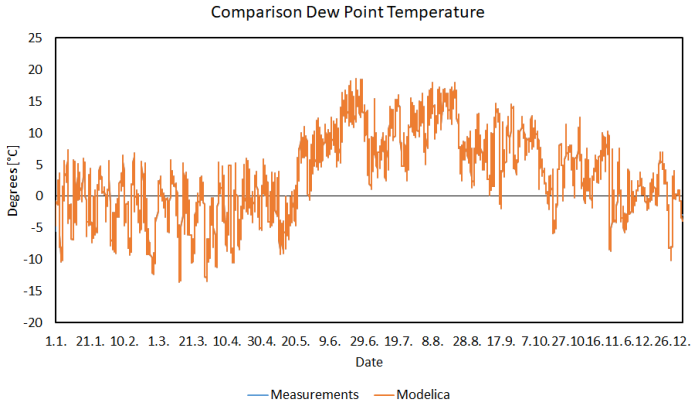

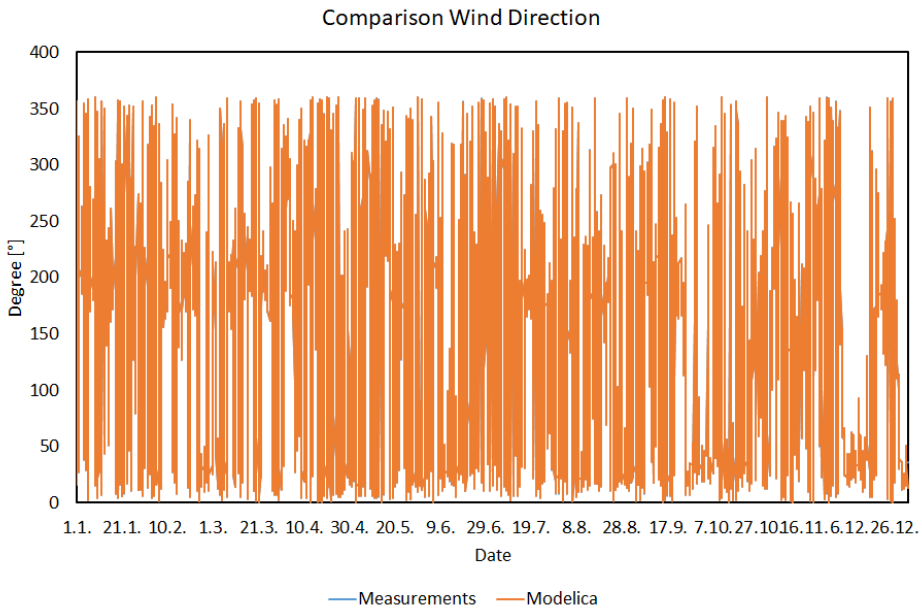
Comparison Wind Direction
400
350
300
250
200
150
100
50
0
Degree [°]
1.1. 21.1. 10.2. 1.3. 21.3. 10.4. 30.4. 20.5. 9.6. 29.6. 19.7. 8.8. 28.8. 17.9. 7.10. 27.10. 16.11. 6.12. 26.12.
Date
Measurements
Modelica

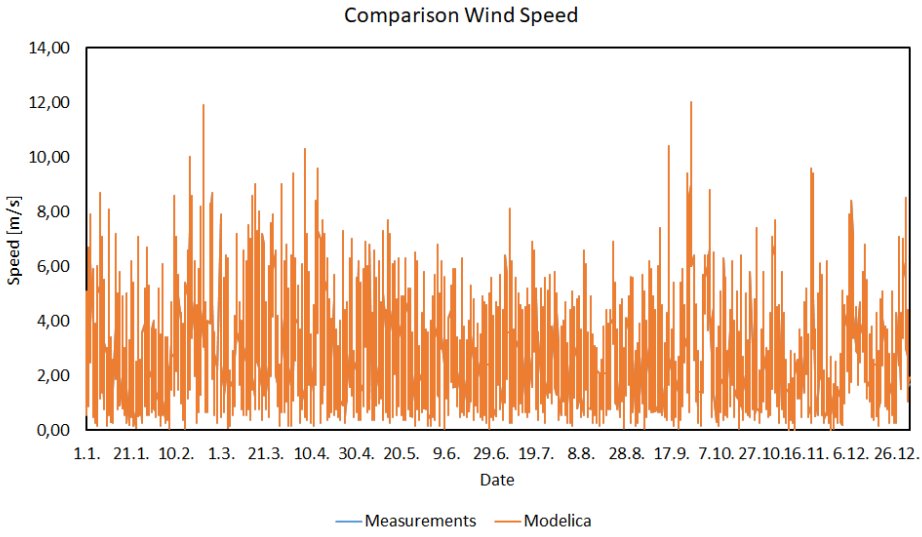
Comparison Wind Speed
14,00
12,00
10,00
8,00
6,00
4,00
2,00
0,00
Speed [m/s]
1.1. 21.1. 10.2. 1.3. 21.3. 10.4. 30.4. 20.5. 9.6. 29.6. 19.7. 8.8. 28.8. 17.9. 7.10. 27.10. 16.11. 6.12. 26.12.
Date
Measurements
Modelica

Appendix C

Overview of the Hydronic Heating Systems for Evaluation of Control Strategies

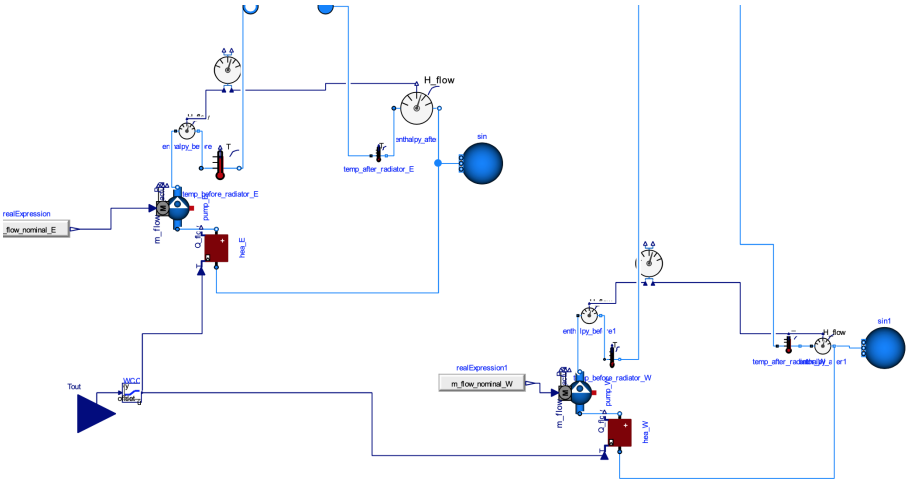

Figure C.1: The hydronic heating system without night setback on the WCC.

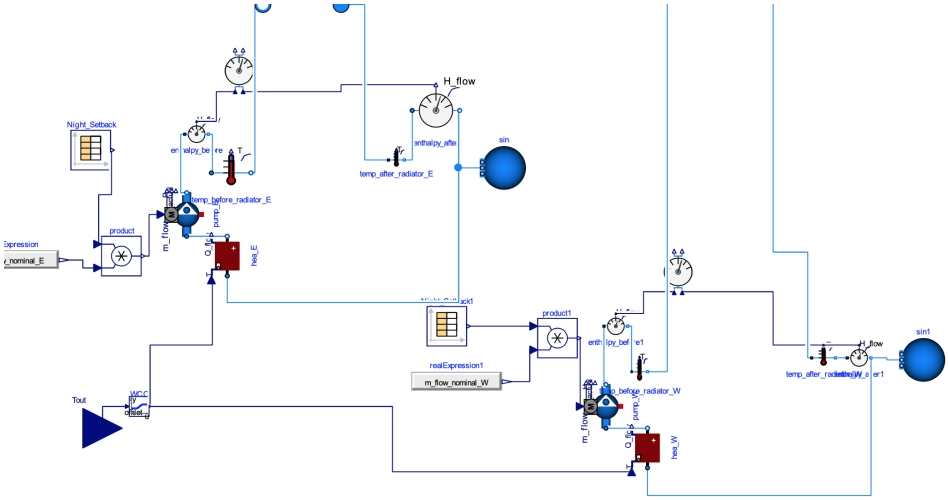

Figure C.2: The hydronic heating system without a night setback on the WCC and night setback on the pump.

Martine Walvik Gundersen

Modelica Emulator for MPC Applications in Buildings

NTNU
Norwegian University of
Science and Technology